Extremum Seeking Control in Ocean Thermal Energy Conversion:

An experimental study

M.A. Terlouw

Master of Science Thesis

TU Delft Delft University of Technology

Delft Center for Systems and Control

Extremum Seeking Control in Ocean Thermal Energy Conversion:

An experimental study

Master of Science Thesis

For the degree of Master of Science in Systems and Control at Delft University of Technology

M.A. Terlouw

April 13, 2018

Faculty of Mechanical, Maritime and Materials Engineering (3mE) · Delft University of Technology

The work in this thesis was supported by Bluerise. Their cooperation is hereby gratefully acknowledged.

Delft University of Technology
Department of
Delft Center for Systems and Control (dcsc)

The undersigned hereby certify that they have read and recommend to the Faculty of Mechanical, Maritime and Materials Engineering (3mE) for acceptance a thesis entitled

Extremum Seeking Control in Ocean Thermal Energy Conversion:

by

M.A. Terlouw

in partial fulfillment of the requirements for the degree of

Master of Science Systems and Control

This thesis is confidential and cannot be made public until April 23, 2023.

Dated: April 13, 2018

Supervisor(s):

prof.dr.ir.Jan-Willem van Wingerden

ir. Bram Harmsen

Reader(s):

Dr.ir. H. Polinder

Ir. S. Mulders

Abstract

Ocean Thermal Energy Conversion (OTEC) is a technique to generate electricity by using the thermal gradient available in the ocean to drive a heat engine. In order for OTEC to become successful it is important to reduce the levelized cost of electricity. The development of an effective control system can aid in this endeavour, by making sure that the plant is always operated at maximum capacity. Theoretically, the optimal control inputs can be determined offline by using models. However, due to modelling assumptions, this method can result in a suboptimal operation of the plant. Besides, performance of the plant varies over time as a result wear and tear, fouling, and fluctuating ocean water temperatures. Comparable obstacles are encountered in maximizing the electricity production in wind turbines. A promising solution in this field is Extremum Seeking Control (ESC). ESC is a model-free control strategy used for the real-time optimization of an unknown objective function. In this study, ESC has been implemented on a room-sized OTEC test-setup, called the OTEC-demo. Single parameter as well as multiparameter ESC algorithms are tested, and are shown to be successful in automatically finding the set of inputs for which the power output of the plant is maximized.

Preface

This report is a part of my Master of Science graduation thesis. The idea of doing my thesis on the subject of Ocean Thermal Energy Conversion came after attending an excursion to the YES!Delft incubator, organized by the Systems & Control study association Out of Control.

First of all I would like to thank ir. Bram Harmsen for his assistance and supervision. With the crowdfunding campaign it were busy times at Bluerise, but you always made time to lend your assistance. Without your expertise this project would have never reached the implementation phase. I would like to thank prof. dr. ir. Jan-Willem van Wingerden for his supervision during this project.

Furthermore I would like to thank my parents. The carefree weekends at home, were and will always be something to look forward to.

I would especially like to thank my dear sister Vera. Your support the last years has been indispensable, and thinking back to our time together in Delft will always bring a smile to my face.

Delft, University of Technology
April 13, 2018

M.A. Terlouw

Contents

List of Figures

"Highly organized research is guaranteed to produce nothing new."
— *Frank Herbert, Dune*

Chapter 1

Introduction

Most renewable energy sources, such as solar and wind energy, are characterized by a relatively low capacity factor. In other words, these plants can not be operated at their maximum capacity since there simply is not enough wind or solar energy available at all times. To match the supply and demand, renewable energy sources like wind turbines and solar panels have to be backed up by power plants, driven by the combustion of fossil fuels. This is not a viable solution for small scale power generation in Small Island Development States (SIDS), due to the high price of imported diesel and oil.

However, in SIDS in tropical regions, there is the potential to generate constant electric power by harvesting thermal energy stored in the ocean. Ocean Thermal Energy Conversion (OTEC) is a technique to generate electricity by utilizing the temperature difference between different depths in the ocean. In this process the warm surface water is used to evaporate a working fluid. The vapour is then led through a turbine-generator, after which the vapour will be condensed again using the cold deep ocean water to complete the cycle.

Roughly 70% of the surface of the earth is covered by oceans [1]. Due to the oceans' low albedo, or reflectance, the majority of the incoming sunlight is absorbed and converted into heat, making the oceans the largest solar collector on the planet. The surface layer is warmed by the sun and mixed by wave activity to a depth of 100m-200m. The deep, colder water originates from higher latitudes and descends along the seafloor to the equatorial regions due to thermohaline circulation [40]. The vertical temperature distribution can be represented by a top- and a bottom layer separated by an interface, also called a thermocline. Figure 1-1 shows the visualization of such a distribution. Assuming a temperature difference ΔT of 20°C between the warm and cold water, the ideal energy conversion efficiency is roughly 8% [40]. An actual plant will achieve a thermal efficiency closer to 3% [40].

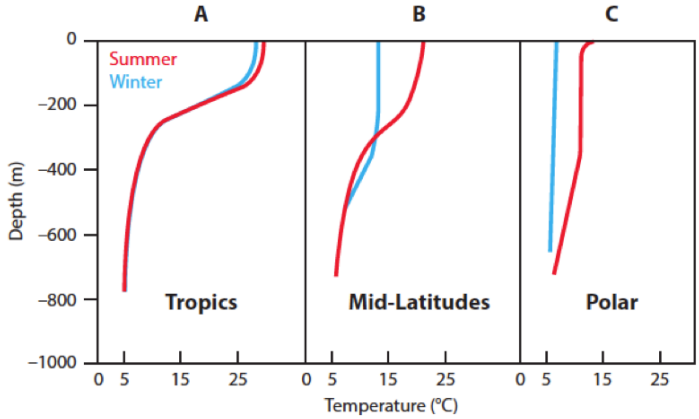

Figure 1-1: Idealized vertical temperature ocean profiles in July and January. Where Figure (A) shows the profile near the equator, (B) at approximately 45° N or S latitude, and (C) near the poles. Courtesy of Byron Inouye

The regions in the world where the surface water temperature is high enough for OTEC purposes are shown in Figure 1-2. In tropical regions the surface layer reaches average year-round temperatures of 28°C. Here the surface ocean temperature is also found to be relatively constant, resulting in a constant power output of OTEC plants. As a result, OTEC has the potential to supply base load power to these regions [9].

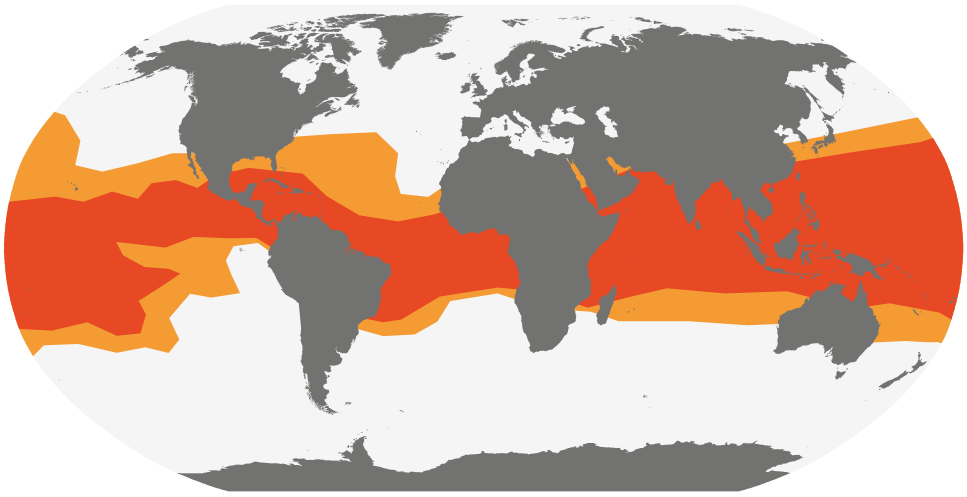

Figure 1-2: Global OTEC resource: light orange depicts a surface water temperature of at least 20 °C, dark orange corresponds to a surface water temperature higher than 25°C, Courtesy of Bluerise B.V.

One of the most important factors to overcome in the succeeding of OTEC as a renewable energy source is reducing the Levelized Cost of electricity (LCOE). The levelized cost can either be reduced by increasing the power output, or by reducing capital and operating costs of the plant. For this purpose, research is being conducted towards working fluid selection, heat exchanger design and turbine design [19]. In addition to improving individual components, entirely new thermodynamic cycles have been developed. At the Delft University of Technology (TU Delft), OTEC research is being conducted in cooperation with Bluerise [4]. The company has developed an advanced room-sized OTEC demonstration plant, called the OTEC-demo.

Besides improving the thermodynamic behaviour of OTEC plants, the development of an effective control system is an important element to consider. The controlled inputs of the plants are the flow rates of the deep ocean water and warm surface water. Variable speed water pumps are used to continuously supply the plant with warm and cold water. Increasing the water flow rates will increase the power output of the turbine, but increases the power consumption of the pumps as well. Due to low thermal efficiency of OTEC plants, large water flows are required. At a ΔT of 20°C, a warm sea water flow of approximately 5 m^3/s and 2.5 m^3/s of cold seawater, is needed for every MW of electricity [40]. As a result, the power consumption of the water pumps is roughly 30% of the total power generated in the turbine [40]. Literature has shown that optimal flow rates exist where the net generated power is maximized [47]. In most OTEC plants, as well as in the OTEC-demo, the controllers follow a fixed reference. To find the optimal inputs, a mapping between the water flow rates and the power yield can be made offline using a model. Determining the optimal sets of inputs using this method is not a straightforward task, due to the following reasons:

- Modelling assumptions can possibly lead to an offset to the optimal set of inputs.
- Parameters of the model can be difficult to determine, and they can vary over time as a result of wear and tear of mechanical components, or for example due to fouling on the heat exchangers [13].
- Accurate measurements of the ocean water temperature are required [47].

Comparable issues are encountered in maximizing the power yield of wind turbines [6]. A promising solution in this field is Extremum Seeking Control (ESC). ESC is a control strategy used for the real-time optimization of an unknown objective function. Besides wind energy, ESC has also been applied in fields closely related to OTEC, such as Organic Rankine and vapor compression cycles [34], [8], [45], [10], [20], [12] , [15]. At the time of writing, ESC has not yet been applied to OTEC. The existing OTEC-demo control system is capable of regulating the mass flows, and measuring the power output in real-time. Hence, ESC-algorithms can be implemented and tested on the OTEC-demo. The controller is proved to be able to optimize the two inputs corresponding to the warm and cold water flow rates, hereby demonstrating the effectiveness of ESC in OTEC. Due to the relatively simple structure of ESC, the controller can be implemented in future projects by Bluerise.

This report is organized in the following manner: Section 2 describes the thermodynamic cycle under study. Section 3 presents the mathematics behind extremum seeking control, and how the algorithm is implemented in the OTEC-demo. The experimental results are given in section 4. Finally, concluding remarks and recommendations are given in the last section.

Chapter 2

System Description

The purpose of OTEC is to convert the energy 'stored' in the ocean to usable electrical energy. This is realized by implementing a thermodynamic cycle. A cycle suitable for OTEC is the so-called Kalina cycle. This advanced cycle is described in the next section. The second section provides an overview of the inputs, outputs and disturbances of the system. With the controlled inputs being defined, the third section describes OTEC control techniques found in the literature. The final section explains how Bluerise has implemented the Kalina cycle in the OTEC-demo.

2-1 Kalina Cycle

In the 1980's A.I. Kalina proposed a thermodynamic energy cycle using a working fluid consisting of a mixture of two components with different boiling points, also known as a binary working fluid [18]. This cycle was designed to replace the currently used Rankine Cycle, especially when using low-temperature heat sources. Since then, several adaptations have been made to the original Kalina cycle, of which an overview is given in the extensive literature survey by Zhang, He, and Zhang [48]. The different cycles are suitable for different operating temperatures. The cycle implemented in the OTEC demo is the so-called KCS 34 g cycle, which is most suitable for small scale plants in combination with heat sources up to 121°C [30]. A schematic overview of the Kalina cycle is shown in Figure 2-1.

The cycle consists of the following processes:

Process 1-2: Pump increases working fluid pressure

Process 2-3: Preheating of the working fluid by the recuperator

Process 3-4: (Partial) evaporation of working fluid in heat exchanger in combination with warm sea water

Process 4-4r/4w: The separator separates the working fluid in liquid and vapor parts

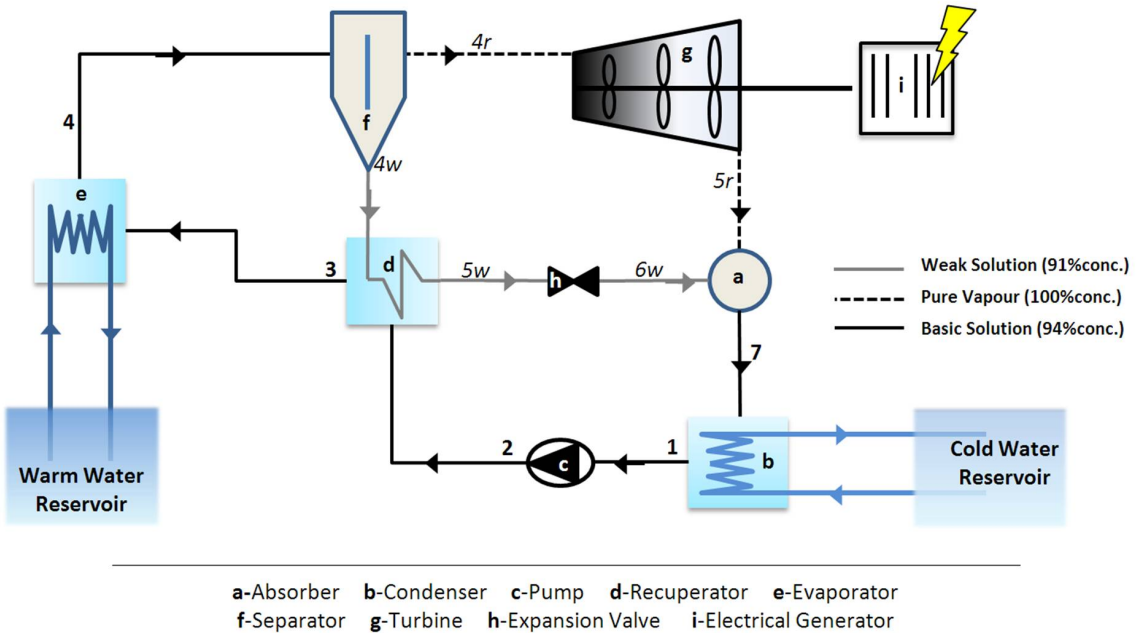

Figure 2-1: Advanced OTEC Cycle, courtesy of Bluerise B.V.

Process 4r-5r: Work is produced in the turbine by means of expansion of the working fluid

Process 4w-5w: The relatively warm liquid preheats the working fluid in the recuperator

Process 5w-6w: Working fluid is expanded through an expansion valve to the same pressure as the working fluid in *5r*

Process 5r/6w-7: The liquid and vapor is mixed in an absorber

Process 7-1: The working fluid is condensed in a heat exchanger fed with cold seawater

2-1-1 Inputs, disturbances and performance

The main actuators in the Kalina cycle are the two water pumps and the working fluid pump. One water pump is used in Process 3-4 to supply the evaporator with warm surface water, and the other pump is used in Process 7-1 to supply the condenser with cold deep ocean water. The working fluid pump, component *c* in Figure 2-1, is used to circulate the working fluid. Another important component is the turbine-generator used in Process 4r-5r. In this study, the performance of the plant is expressed by the net generated power. The net generated power in the cycle equals the power generated in the turbine, minus the power consumed by the pumps. As a result of the small temperature difference between the surface water and deep ocean water, OTEC plants inherently suffer from a low thermal efficiency [40]. Due to this low thermal efficiency, the required water flows are significant. Both hot and cold flows are in the order of 5 m^3/s for every MW of generated electricity. As a result, the power consumption of the pumps accounts for roughly 30% of the total power output [41].

The net power is given by:

$$W_{net} = W_{Turb} - \sum W_{Pump} \tag{2-1}$$

Here, the power consumption of auxiliaries such as the control system itself, is neglected.

Vapour expands through the turbine, hereby causing the turbine blades to rotate. The shaft work of the turbine is then converted to electrical energy by means of a generator. The power converted by the turbine-generator system is given by:

$$W_{Turb} = \dot{m}_t \ \eta_t \ (h_{t,i} - h_{t,o}) \tag{2-2}$$

Where $\dot{m}_t$ corresponds to the mass flow of the working fluid through the turbine, η_t the isentropic efficiency of the turbine and generator. $h_{t,i}$ and $h_{t,o}$ are the working fluid enthalpies at the in-and outlet of the turbine, respectively.

The power consumption of a pump is given by:

$$W_{Pump} = \frac{\dot{m}_p \ g \ \Delta P_{ws}}{\eta_{ws}} \tag{2-3}$$

Where $\dot{m}_p$ is the mass flow rate, g the gravitational constant, ΔP_{ws} is the pressure difference encountered in the pipe and η_{ws} describes the isentropic efficiency of the pumps.

2-1-2 Control-oriented Schematic

The inputs, disturbances and output of the system are visualized in Figure 2-2. The inputs u_1 and u_2 are the control signals of the warm and cold water pumps. Where increasing the control signal u_1 will increase the warm water flow rate $\dot{m}_w$, an increase in u_2 results in an increased cold water flow rate $\dot{m}_c$. In this study, the working fluid pump speed is kept constant, this choice is further motivation in Appendix A-2. The disturbances T_h and T_c are the temperature of the warm surface water and deep ocean water. The literature investigates the influence of other disturbances, such as wave activity influencing the inlet pressure at the warm water pipe [33]. These disturbances are difficult to simulate in the OTEC-demo, and are thus not analysed in this report. The performance of the plant corresponds to the net generated power W_n, as calculated in Equation 2-1.

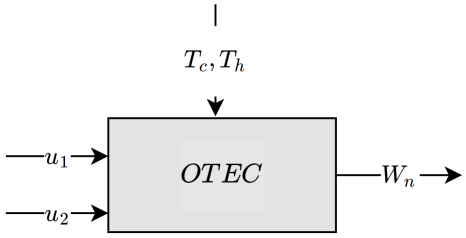

Figure 2-2: Control-oriented schematic of the OTEC process

2-1-3 Control in OTEC

The first available publication on control of OTEC plants dates back to 1982 [33]. In this work, the use of variable seawater pumps to control the output power is suggested. Owens suggests that the optimal power output and corresponding mass flow rates can be determined by measuring seawater temperatures, heat exchanger fouling, line losses and equipment efficiencies. However, details on this optimization process are not given. Comparable optimization procedures that are only based on measurements of the ocean water temperatures, are found throughout literature [35], [38], [43]. These methods do not take time the varying behaviour of fouling and equipment efficiencies into account.

Goto et al. used system identification techniques based on step-responses of an OTEC plant to obtain a model between water flow rates and the output power. The nonlinear separation controller built using this model is shown in Figure 2-3. The upper control system is used to map W_{ref} to flow rates of warm water, cold water and working fluid. These flow rates are then regulated by the lower level control system, consisting of PI controllers. The tracking performance of this control strategy depends on the quality of the nonlinear separation model.

In a more recent study, Matsuda et al. demonstrated that PI-controllers are also capable of tracking a reference output power of a model OTEC plant [29]. Disturbances were considered in the form of fluctuations in the warm water temperature. Figure 2-4 shows that the offset to W_{ref} is directly used as input of the PI controllers, and that no mapping between W_{ref} is needed to gain adequate tracking performance.

It is important to note that these control systems have been tested using simulations, and are yet to be implemented in actual plants. At the time of writing, only a few OTEC plants are operational worldwide and details on their control systems are scarce. Apak et al. briefly describes the control system of Mini-OTEC, a test plant that was built at the end of the 1970's [2]. The control system was capable of tracking manually determined references corresponding to the water flow rates. In Húsavík, Iceland, a geothermal power plant is built based on the Kalina cycle. The control strategy of this plant is also used to track flow rates, in this case of the hot brine [16].

2-1-4 Optimal Performance

As mentioned, the maximum attainable power output of an OTEC plant is limited by the available temperature difference between the warm and cold ocean water. For a given temperature difference, the output power of an OTEC plant can be controlled by regulating the water flow rates. In literature, static models are used to investigate the performance of OTEC plants [47], [43], [36], [44]. Based on such a model, Yeh, Su, and Yang demonstrate that there exists an optimal cold water flow rate that maximizes the net power production of a 1MW ORC-based plant [47].

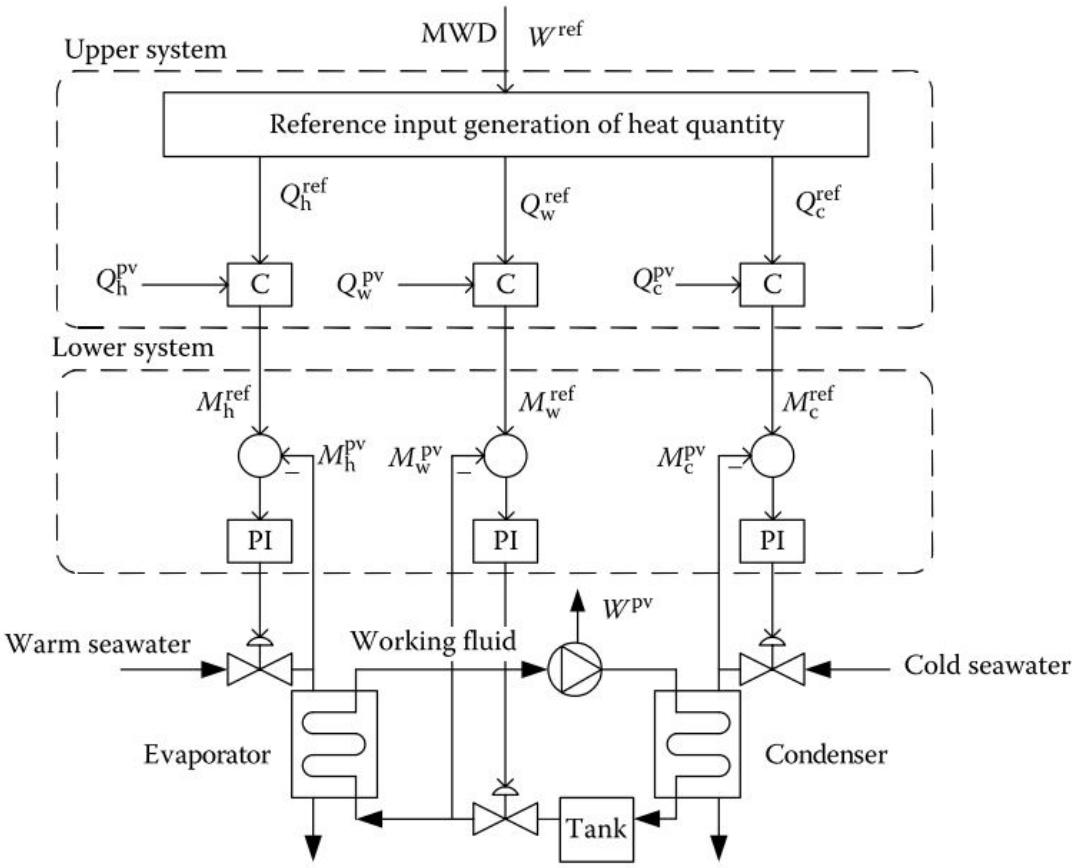

Figure 2-3: Nonlinear separation controller [11]

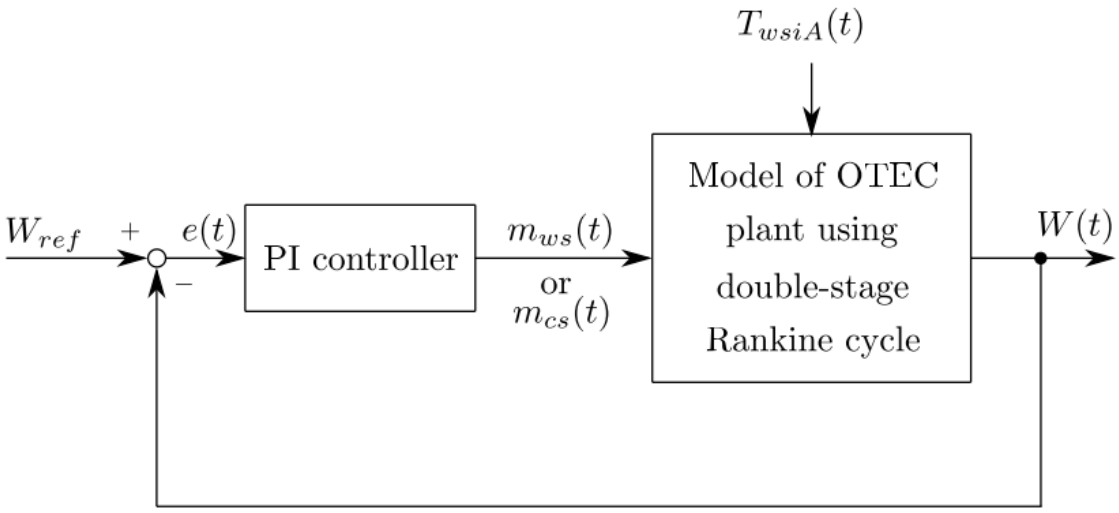

Figure 2-4: Reference tracking using PI-controllers [29]

As shown in Figure 2-5a, the power output of the turbine increases by increasing the cold water flow rate, albeit at a decreasing rate. At the same time, the power consumption of the cold water pump increases at an accelerating rate. As a result, the net generated power assumes a parabolic shape, with an optimal net power output of roughly 250kW for a cold water flow rate of approximately 3000 tons/hr.

Figure 2-5b shows that the optimal flow rate depends on the deep ocean water temperature. A 1 °C increase in the cold water temperature results in a decrease in the net power output of roughly 20%. Even more if the cold water flow rate would not be adjusted accordingly. Thus, to operate an OTEC plant at maximum capacity, accurate measurements of the ocean water temperature are needed. Figure 2-6 shows that the water temperatures vary considerably, even within the timespan of an hour. The temperature fluctuations are measured in the vicinity of a 210kW experimental OTEC plant [39]. The effect of the varying water temperatures on the power output of this plant is also visualized in Figure 2-6.

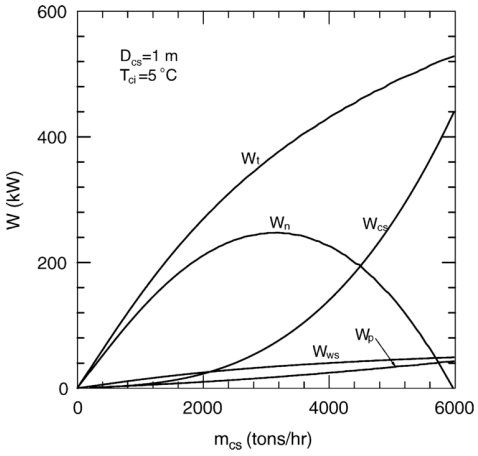

(a) Power generation and consumption for different flow rates of cold water

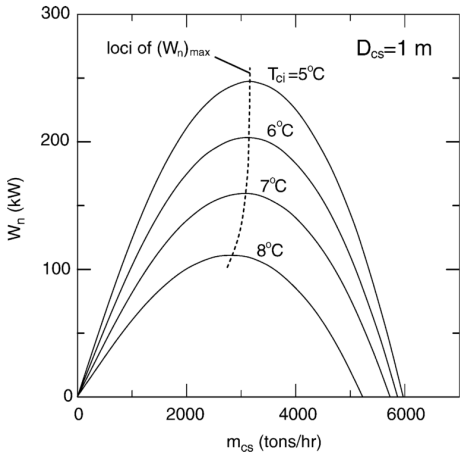

(b) Net Power production as a function of cold water flow rates for different DOW temperatures

Figure 2-5: Dependence of W_n on flow rates and temperatures [47]

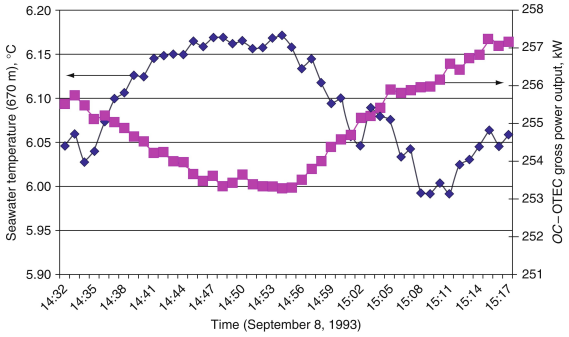

(a) Deep Ocean Water temperature fluctuations

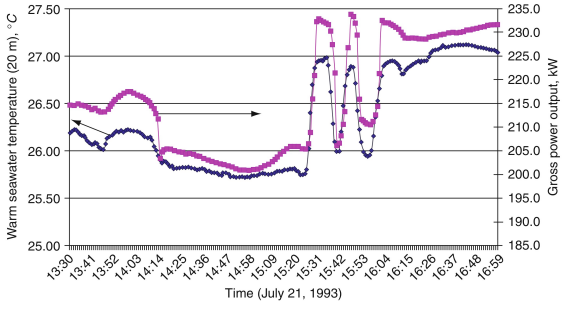

(b) Surface water temperature fluctuations

Figure 2-6: Water temperature and power output of a 210kW OTEC plant [40]

2-2 OTEC-demo

In cooperation with the Delft University of Technology, Bluerise has developed an advanced OTEC test-setup [14]. The so-called OTEC-demo is used to investigate the effect of different water temperatures and flow rates, working fluid compositions, and since recently also different heat exchangers configurations [7], [24]. The working fluid composition expresses the ratio between water and ammonia. During this study the working fluid in the OTEC-demo consisted of 100% ammonia. Figure 2-7 shows the test-setup in its current state of development. The red numbers indicate the most important components: Number 1,2 and 3 indicate the pumps for warm water, cold water and working fluid. 4 shows the location of the turbine. Numbers 5,6 and 7 indicate the evaporator, condenser and recuperator.

Figure 2-7: The OTEC demo test-setup, courtesy of Bluerise B.V.

2-2-1 Inputs

In the test setup, the flow rates of working fluid and water can be adjusted in either a closed-loop or open-loop fashion. Using the closed-loop method, a mass flow rate is tracked using PI-controllers. In the open-loop method, the pumps are operated at a fixed control input. The control signals of the warm and cold water pump, indicated by u_1 and u_2 in Figure 2-2, are expressed in percentages of the maximum pump frequency. The pumps can be operated in a range between 20Hz and 50Hz, hence 1% in the control signal corresponds to 0.3Hz. Due to the boundedness of the control signal, the operating range of the water pumps lies between 0.1 and 1.0 L/s.

2-2-2 Performance

At the time of writing, the demo is not fitted with an actual turbine. Hence, there is no electricity being generated during operation of the system. However, the functioning of a turbine is simulated by means of an orifice. The hypothetical power generated over this orifice, would it be replaced with a turbine, can be estimated [24]. The hypothetical turbine power is given by:

$$W_{Turb} = \eta_{is}\ \dot{m}_t\ c_p T_{in} \left(1 - \frac{P_{turb,out}}{P_{turb,in}}\right)^{\frac{\gamma-1}{\gamma}} \tag{2-4}$$

Note that Equation 2-4 corresponds to mechanical power, and not to electrical power. The quantities in Equation 2-4 can be measured directly, and do not require the real-time evaluation of working fluid properties, as would have been the case when Equation 2-2 would be used. The efficiency η_{is} is assumed to be equal to 1. $P_{turb,in}$ and $P_{turb,out}$ are the pressures at the inlet and outlet of the turbine, and T_{in} is the inlet temperature. The working fluid properties c_p and γ are considered as constants, and are determined using a temperature of 25 °C.

The power consumption of the water pumps is calculated using Equation 2-3, assuming a fixed efficiency of 0.4. Measurements showed that the output of one of the pressure sensors in the warm water pipe suffered from significant amounts of noise. In Appendix A is shown how a third order polynomial is fitted that directly relates the power consumption of the two water pumps to their control signal u_1 and u_2. The power consumption of the water pumps is now determined without requiring measurements of the pressure drop. As a result, Equation 2-3 is reduced to:

$$W_P = f(u_n) \tag{2-5}$$

Note that this only holds for the power consumption of the water pumps. The power consumption of the working fluid pump can not be considered to be independent from the water flow rates. Hence, the working fluid pump power consumption will still be evaluated using Equation 2-3.

As stated in Equation 2-1, the net power can be calculated by subtracting the power consumption of the pumps from the power generated in the turbine. The net mechanical power in the OTEC-demo is obtained by subtracting Equation 2-5 and Equation 2-3 from Equation 2-4, resulting in the following function:

$$W_n = \eta_{is}\ \dot{m}_t\ c_p\ T_{in}\left(1 - \frac{P_{turb,out}}{P_{turb,in}}\right)^{\frac{\gamma-1}{\gamma}} - \frac{m_p\ g\ \Delta P_{wf}}{\eta_{ws}} - f(u_1) - f(u_2) \tag{2-6}$$

As a result, the performance of the OTEC-demo depends on the following measured states:

$$x = [\dot{m}_T, \dot{m}_P, T_{in}, P_{turb,in}, P_{turb,out}, P_{wf,in}, P_{wf,out}, u_1, u_2] \tag{2-7}$$

Where the mass flows are expressed in kg/s, temperature in °K, pressures in Pa and control signals in %. The subscripts 1 and 2 of the control signals correspond to the warm water pump and the cold water pump, respectively.

2-2-3 Disturbances

In contrast to actual OTEC power plants, the OTEC-demo allows the water temperatures to be controlled. Previous experiments by Bluerise students and employees have been performed at $T_c = 5°C$ and $T_h = 27°C$. For comparability purposes, these temperatures are also used during the experiments in this study.

2-3 Discussion

The energy stored in the ocean can be converted by means of a thermodynamic cycle. The controlled variables of such a system are the flow rates of the warm and cold ocean water. These flow rates can be varied by using variable speed pumps. The net output power is considered an important measure of performance for OTEC systems. The net generated power is calculated by subtracting the power consumption of the pumps from the power generated by the turbine.

Examples from literature demonstrate that the net output power can be controlled by regulating water flow rates of the system. Using simulation studies, model-based controllers as well as PI controllers are found to be suitable for tracking a reference power output. Literature shows that there exists an optimal cold water flow for which the net power is optimized. The optimal water flow rate and corresponding net power output depend on the deep ocean water temperature. The ocean water temperatures are shown to vary in time. As a result, continuous optimal plant operation would require accurate measurements of the water temperature, and a mapping between the water flow rate, measured temperature and power output.

The discussed control systems have been developed using simulation studies, but are yet to be implemented in actual OTEC plants. The OTEC-demo allows control over the flow rates and temperatures, and is fitted with numerous sensors to evaluate the performance for all these different inputs. Hence, the OTEC-demo is an excellent tool to develop more advanced control systems than that are currently in use in OTEC.

Chapter 3

Extremum Seeking Control

The introduction emphasized that for OTEC power plants to become commercially attractive, it is necessary to decrease the price of electricity they generate. An effective control system can contribute to this goal by enabling the plant to always be operated at maximum capacity. Chapter 2 demonstrated that there exists an optimal cold water flow, for which the net output power of an OTEC power plant is optimized. Theoretically, the optimal water flow rates can be determined using a model of the plant. However, the OTEC process is difficult to model, especially when an advanced cycle such as the Kalina Cycle is used. Additionally, the characteristics of the plant can also change over time, for example due to wear and tear of the water pumps and fouling on the heat exchangers [1]. It was also found that the optimal water flow rate depends on the cold water temperature, and that this temperature varies throughout the day [47], [40]. Thus, continuous accurate measurements of the water temperatures would be required to keep the plant operating optimally.

Comparable challenges are encountered in optimizing the energy capture of wind turbines [6]. Here, the energy capture can be maximized by controlling the pitch and rotor speed [17]. As with OTEC, a power map between the two controlled inputs and the power output can be made using models. The aerodynamic interactions between the wind and the blades of the turbine are again difficult to model accurately, and often do not take into account time-varying characteristics of the turbine [6]. And where the optimal operation of an OTEC plant requires the water temperatures to be measured, this wind turbine control method requires a measurement of the wind speed [23].

A solution that omits the need of a power map and measurements of the disturbances, is found in a control strategy called Extremum Seeking Control (ESC). Recently, ESC has succesfully been applied in the optimization of electricity production in variable speed wind turbines and wind farms, by automatically finding the optimal set of inputs [34], [8], [45], [10], [6].

Labar, Garone, and Kinnaert provide the following definition of extremum seeking:

> *'Non model-based extremum seeking is a well known control strategy to steer a system to optimize the steady state cost, without requiring the knowledge of the cost function or the system dynamics.' [25]*

In OTEC, the cost function is the power map between the water flow rates and the net generated power. And indeed, due to the obstacles encountered in modelling and the cumbersome activity of manually determining the power map on the plant itself, the cost function and plant dynamics can be considered unknown. What is important however, is that the value of the cost function can be measured for different inputs. That this is indeed the case for the OTEC-demo is discussed in section 2-2-2, where the net output power of the OTEC-demo is expressed in measurable quantities. Additionaly, for ESC to function properly, it is important that the cost function is concave [32]. This is demonstrated in section 2-1-3, by showing the parabolic relation between the cold water flow rate and the output power of an OTEC plant. For the analysis in this chapter, it is assumed that such an optimum also exists for the warm water flow rate. The existence of an optimal warm water flow will also be demonstrated experimentally in chapter 4.

The next section provides an overview of possible applications of ESC found in literature. The second section explains the mathematics behind the basic ESC scheme. As a proof of concept, ESC is used to find the set of inputs that optimize the output of a paraboloid. In the last section is discusses how ESC can be implemented in LabVIEW.

3-1 Literature Review

ESC-algorithms are divided into two different categories [32]:

- So called probe & observe methods, that add a perturbation signal to the controlled inputs [21].
- Methods that do not require an external probing signal, such as sliding mode ESC, and relay-ESC [32].

The most commonly used algorithms belong to the first category. While the first publications regarding ESC date from the 1920's, the method only recently gained in popularity as a result of a proof of stability by Krstić [21], [26]. To this day, this remains one of the leading works in the field of ESC. While Krstić focuses on sinusoidal perturbation signals, several other signals can be used, such as square and triangular waves, or even Gaussian distributed stochastic signals [37], [28].

Since ESC is aimed at optimization, the control strategy is suitable for Maximum Power Point Tracking (MPPT) in (renewable) energy conversion systems. So has ESC been used to optimize the power output of solar panels by finding the optimal settings for the power converter [46] [27]. Recently, ESC has succesfully been applied in the optimization of electricity production in variable speed wind turbines and wind farms [34], [8], [45], [10]. Here, the controller

is responsible for determining the optimal control torque and pitch angle. ESC has also been succesfully been applied to energy conversion systems more closely related to OTEC, such as vapor compression cycles [20], [12] and the control of Organic Rankine Cycles Organic Rankine Cycle (ORC) [15]. In vapour compression cycles, ESC is used to autonomously discover the optimal inputs that minimize the power consumption, while in the case of ORC control ESC is used to maximize power production.

3-2 The Basic perturbation based ESC-scheme

This section covers the theory behind extremum seeking. The basic algorithm, such as the one covered by Krstić is adapted to OTEC. In short, the goal of ESC is to find a parameter $u \in \mathbb{R}$, such that the performance index $f(u,t)$ reaches an optimal value, or

$$u^* = \underset{u}{\operatorname{argmax}}\, f(u,t)$$

Here, u is the control input, and $f(\cdot) : \mathbb{R}^n \times \mathbb{R}^1 \to \mathbb{R}^1$ is assumed to have a unique global maximum.

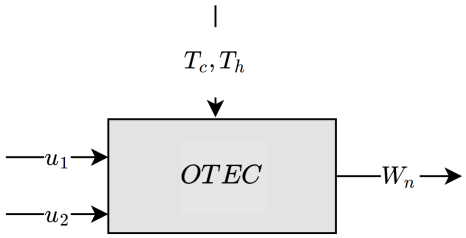

Figure 3-1: Control-oriented schematic of the OTEC process

When applied to the schematic OTEC process, shown in Figure 3-1, ESC is responsible for finding the optimal inputs u_n^*, such that the output power is maximized, or $W_{max} = W_n(u_n^*)$.

The classic multivariable ESC scheme, adapted to OTEC, is shown in Figure 3-2. In this scheme the nonlinear plant is given by:

$$\dot{x} = f(x,u,t) \tag{3-1}$$
$$W_n = h(x,u) \tag{3-2}$$

Where the cost function W_n is equal to the net power output, u is equal to the input signals, and x is a vector that consists of all the relevant internal states of the plant.

The input of the plant is perturbed by a sinusoidal excitation signal $a\sin(\omega t)$, also called *dither*. The perturbed input is given by $u = \hat{u} + a\sin(\omega t)$, with corresponding output $W_n = f(\hat{u} + a\sin(\omega t))$. This expression can be approximated with a Taylor expansion around the estimated gradient $\hat{u}$, resulting in:

$$W_n \approx f(\hat{u}) + \frac{df(u)}{du}|_{u=\hat{u}}\, a\sin(\omega t) + ...$$

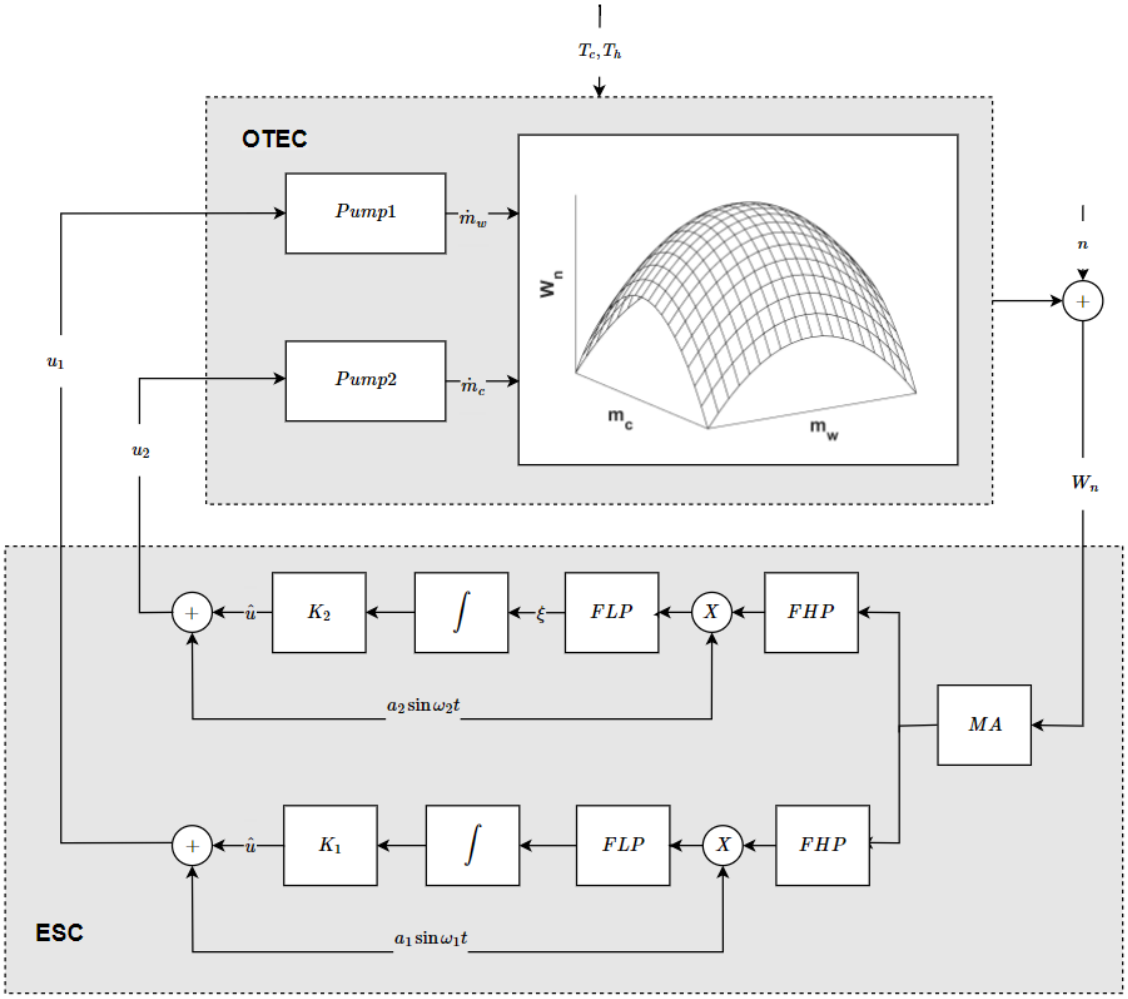

Figure 3-2: Multi variable ESC in OTEC

The output is fed through the high-pass filter. The purpose of this filter is to eliminate the DC-component of the map $f(u^*)$ Assuming a properly chosen cut-off frequency, the filtered output is equal to:

$$y_{hp} = \frac{df(u)}{du}|_{u=\hat{u}} \; a \sin(\omega t)$$

The high-pass filter and the multiplication with the demodulation both serve the purpose of removing the DC-component. Multiplying y_{hp} with the demodulation signal, and using the trigonometric identity $\sin^2(\omega t) = 1 - \cos(2\omega t)$, results in:

$$y_{hp} * M(t) = \frac{df(u)}{du}|_{u=\hat{u}} \; (1 - 2\cos(2\omega t))$$

For an appropiate cut-off frequency, the low-pass filter removes the $\cos(2\omega t)$ component from the signal, resulting in a signal proportional to the gradient. The loop is closed with the

scaled integrator, which serves the purpose of driving the gradient to zero. The speed at which this takes is place is influenced by the adaptation gain k. The MA block is a moving average filter, which is used to deal with measurement noise.

The performance of the basic ESC-algorithm depicted in Figure 3-2 depends on the tuning of five parameters, namely the adaptation gain k, the amplitude a and frequency ω of the dither, and the cut-off frequencies of the low-pass and high-pass filters. Guidelines for tuning of the controller parameters can be found in literature [3]. The guidelines are summarized as follows:

- The dither frequency ω should be slower than the open-loop dynamics of the plant [15]. ω should not be chosen equal to any frequency component present in the measurement noise n. In the case of multivariable ESC, the dither frequencies belonging to different actuators should be distinct [42]. Increasing ω allows the adaptation gain k to be increased proportionally.
- The dither amplitude a is to be chosen small enough that the oscillations in the steady-state output are of acceptable amplitude. The smaller a, the smaller the offset to the optimum is. However, decreasing a will also reduce the quality of the estimated gradient, and hereby reducing the signal-to-noise ratio of the measured cost function [31].
- Increasing the adaptation gain k will increase the speed of adaptation [22]. Increasing k also increases the influence of noise present in the output of the low-pass filter, which introduces an upper limit to the value of k.
- Typically, the cut-off frequencies can be chosen equal to the dither frequency [20].

3-3 Proof of Concept

For demonstration purposes, ESC is used to find the inputs that maximize the output of the following paraboloid:

$$y = -0.02(u_1 - 35)^2 - 0.07(u_2 - 45)^2 + 250 \tag{3-3}$$

3-3-1 Single Parameter ESC

The cost function y reaches a maximum value of 250 for $u_1 = 35$ and $u_2 = 45$. To test the algorithm for a single parameter, u_2 is fixed at 45. The cut-off frequencies off the filters are set equal to the dither frequency ω. Figure 3-3a shows the control signal and corresponding value of the cost function y. The figure shows that the trajectory converges in roughly 400s. The speed of adaptation is found to be very sensitive to the adaptation gain k. In Figure 3-4a is shown that merely changing k from 0.0029 to 0.0025 and 0.0034 increases the convergence time to more than 25000s.

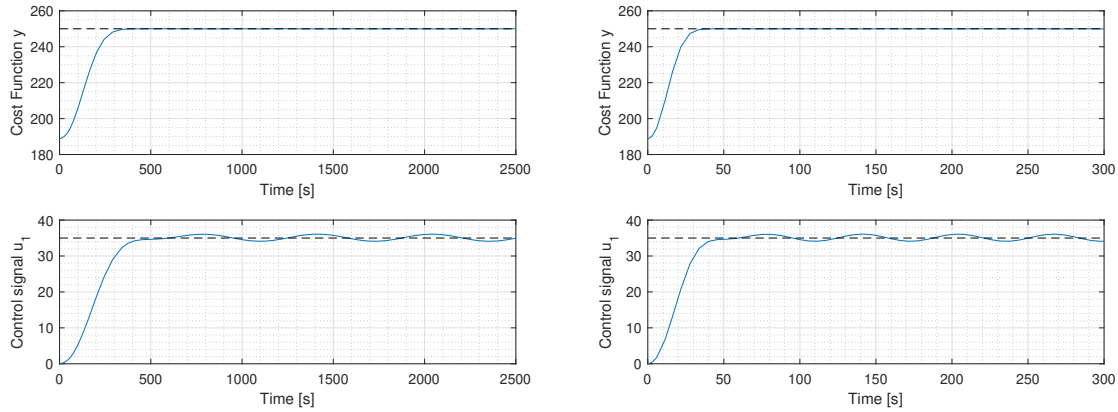

(a) ESC for fixed u_2, $a = 1$, $\omega = 0.01$, $k = 0.0029$ **(b)** ESC for fixed u_2, $a = 1$, $\omega = 0.1$, $k = 0.029$

Figure 3-3: Influence of dither frequency on the speed of convergence

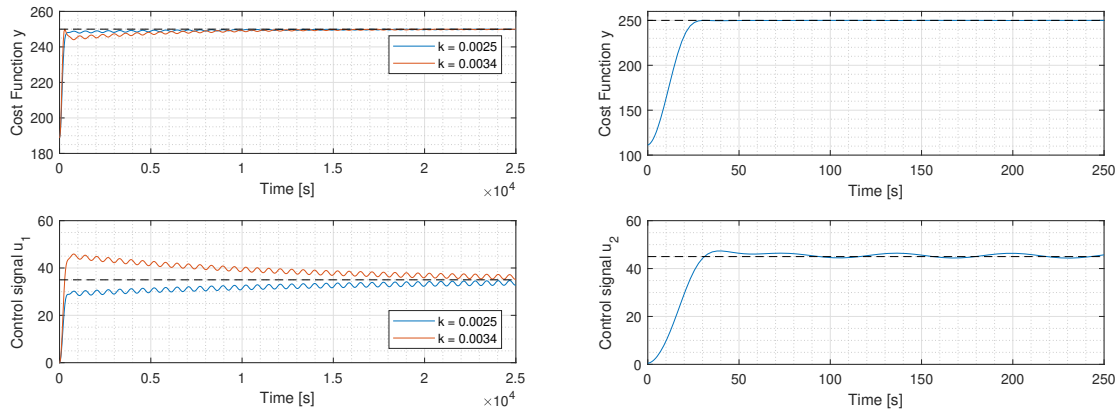

(a) Single Parameter ESC for fixed u_2, $a = 1$, $\omega = 0.01$ **(b)** Single Parameter ESC for fixed u_2, $a = 1$, $\omega = 0.1$, $k = 0.037$

Figure 3-4: Influence of dither frequency on the speed of convergence

The speed of of convergence also depends on the dither frequency ω. Increasing w allows the adaptation gain k to be increased proportionally. Increasing ω to 0.1 and k to 0.029 results in the response shown in Figure 3-3b. Increasing w and k by a factor ten has reduced the time until convergence to roughly 50s.

The single parameter algorithm has also been used to find the optimal value of u_2 when u_1 is fixed at 35. The response is shown in Figure 3-4b. For $k = 0.037$ the controller converges to the optimum in approximately 100s.

3-3-2 Multivariable ESC

ESC can also be applied to optimize u_1 and u_2 simultaneously. Figure 3-5 shows how both inputs converge to their optimal values in approximately 500s. The adaptation gains needed

to be tuned again to obtain the desired response. Note how both dither signals have distinct frequencies. The trajectories of u_1 and u_2 can also be visualized in a contour plot, as shown in Figure 3-6. Here, the contour is described by the paraboloid from Equation 3-3. The red line indicates the trajectories of both inputs. Starting from point (0,0) the input signals converge to a region around the optimum (35,45).

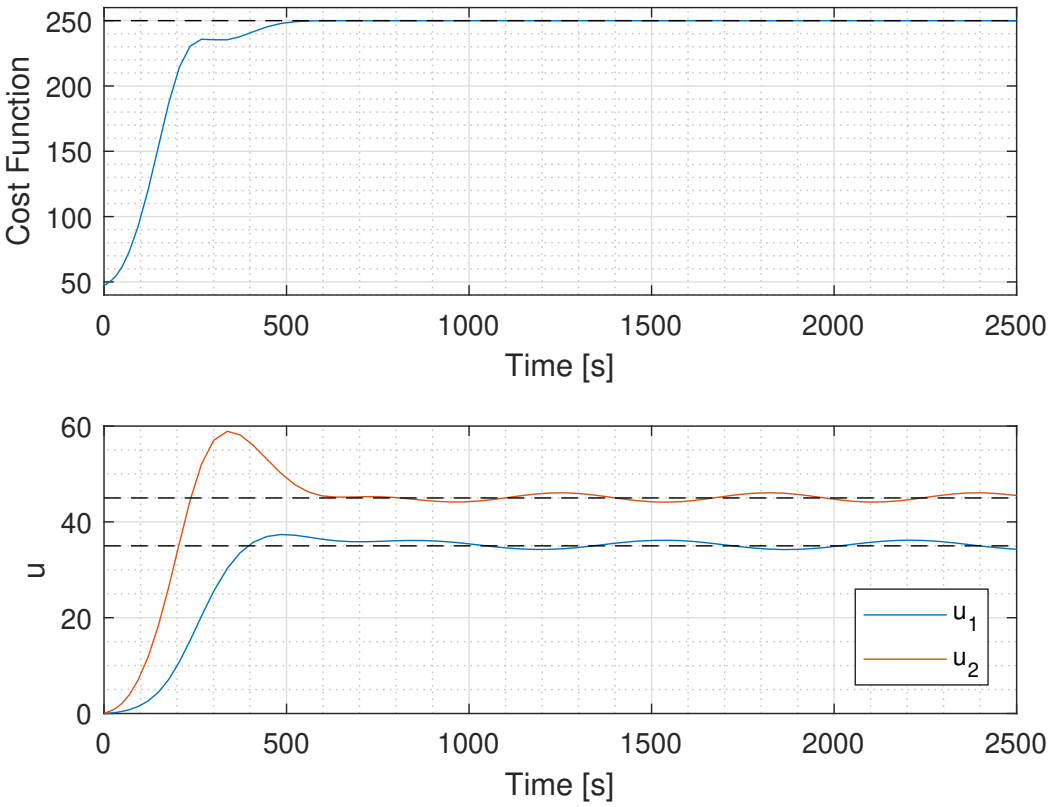

Figure 3-5: Multivariable ESC with $a_{1,2} = 1$, $\omega_1 = 0.093$, $\omega_2 = 0.011$, $k_1 = 0.0028$, $k_2 = 0.0074$

3-4 LabVIEW Implementation

The OTEC-demo is equipped with an advanced operating system based on LabVIEW. The operating system interacts with National Instruments CompactRIO (cRIO) controller with additional I/O modules [14]. The ESC-algorithm is added as an additional Virtual Instrument (VI). The control system is designed so that the different tuning parameters can be changed easily. The filters can be switched on and off individually, and the operator can switch quickly between the different actuators, making the system suitable for single variable, as well as multivariable ESC. Appendix A shows how a useful measurement of the cost function is obtained in the OTEC-demo.

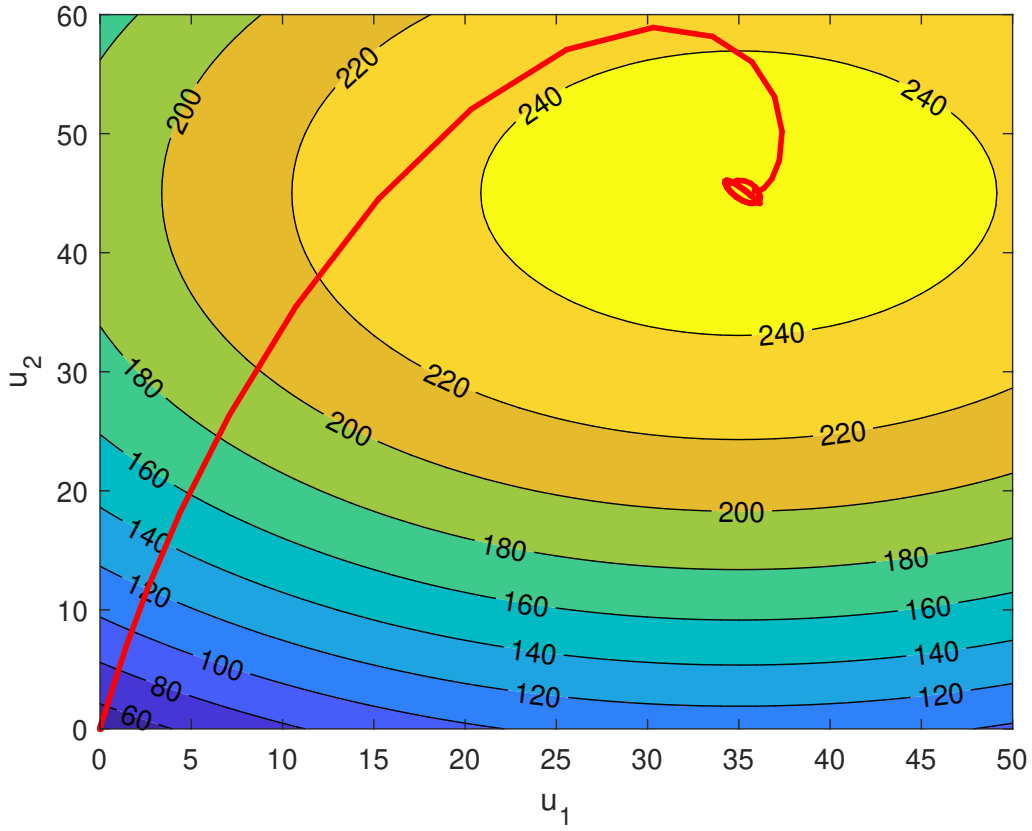

Figure 3-6: Trajectories of multivariable ESC

3-5 Discussion

In the first two chapters was emphasized how the net output power of an OTEC plant can be optimized by finding an optimal water flow rate. The exact mapping between the flow rates and the power output is difficult to obtain, due to the complex thermodynamic cycle used in OTEC. A comparable challenge is faced when maximizing the power output of wind turbines. In this field, ESC was found to be a promising solution. Due to the concave relation between the cold water flow rate and the power output in OTEC, ESC is also expected to be applicable in this field.

As a proof of concept, a multivariable ESC-algorithm is used to determine the set of inputs that maximize the output of a paraboloid function. By fixing one of the input signals, single parameter ESC is tested. By using two ESC loops, both inputs can be optimized simultaneously. Based on the simulation study can be concluded that the ESC-algorithm is successful in finding the optimal inputs. The controller is found to be very sensitive to the values of the adaptation gain and dither frequency.

By step-by-step increasing the water flow rates in the OTEC-demo, the optimal inputs and corresponding outputs can be evaluated. The ESC-algorithm can be considered effective when it is able to automatically find the same optimal inputs. Extremum seeking controllers

consist of simple building blocks, such as low-pass filters, high-pass filters, and an integrator. As a result, the controllers can easily be implemented in the LabVIEW control system of the OTEC-demo, or in the control system of a full-scale plant.

Measurement noise and dynamics of the system were not taken into account in the proof of concept. As a result, the adaptation gain and dither frequency can be increased indefinitely. The speed of adaptation in the OTEC-demo will be limited by the signal-to-noise ratio of the measured cost function. How the signal-to-noise ratio of is improved, is discussed in Appendix A.

Chapter 4

Results

This chapter provides an overview of the experimental results. In section 2-1-3 is shown how the power output of an OTEC power plant is optimized for a specific flow rate of cold water. During the first experiment is investigated whether such an optimum also exists for the warm water flow rate in the OTEC-demo. In the second experiment, a power map between the two flow rates and the output power is constructed. Using the power map, optimal control signals and corresponding power outputs are estimated. Then, single parameter and multivariable ESC are tested. The algorithm is validated by comparing the steady-state values from the ESC experiments with the estimated optimal values.

To recap, the two control signals, u_1 and u_2, control the pumping speed of the warm water pump and cold water pump, respectively. The performance of the OTEC-demo, expressed by the net mechanical power output W_n, is calculated using Equation 2-6. The trajectory of this cost function depends, among other things, on the temperature of the hot and cold water, or T_h and T_c. These temperatures are controlled in the OTEC-demo, and set to 27 °C and 5 ° C. The power 'generated' in the orifice is calculated using Equation 2-4.

4-1 Step-Response

The control signal of u_1 is increased in increments of 5%. By increasing the flow rate of warm water, more energy is transferred to the working fluid. In turn, this will lead to an increase in the amount of vapour passing through the orifice, and thus an increase in power output. On the other hand, increasing the warm water flow rate also increases the power consumption of the corresponding water pump. This first experiment serves two purposes; second-order models can be fitted to the step-response, these are then used to approximate the bandwidth of the system and finally to determine a suitable dither frequency ω. By increasing the mass flow rate step-by-step, the optimal value of the control signal and corresponding net power generation can be estimated manually. This data can then be used to verify whether the ESC-algorithm is indeed converging to the global optimum.

4-1-1 Step-Response u_1

As a first experiment, the control signal u_2 is kept constant at 10%, while the control signal u_1 is increased in steps of 5%, until an input of 50% is reached. A step is observed until W_n has appeared to reach a steady-state, based on inspection of the real-time data feed. Judging by the results shown in Figure 4-1, it is clear that W_n reaches a maximum value of roughly 180W around the 550s mark, for a control signal u_1 between 20% and 25%. The turbine power keeps increasing over the entire range of the input, albeit it at a decreasing rate. This first experiment demonstrates that there indeed exists a unique warm water flow rate and corresponding control signal u_1 that maximizes W_n of the OTEC-demo. In the next experiment, u_2 is also varied, in order to investigate whether such an optimum also exists for different combinations of inputs and to construct a three dimensional power map.

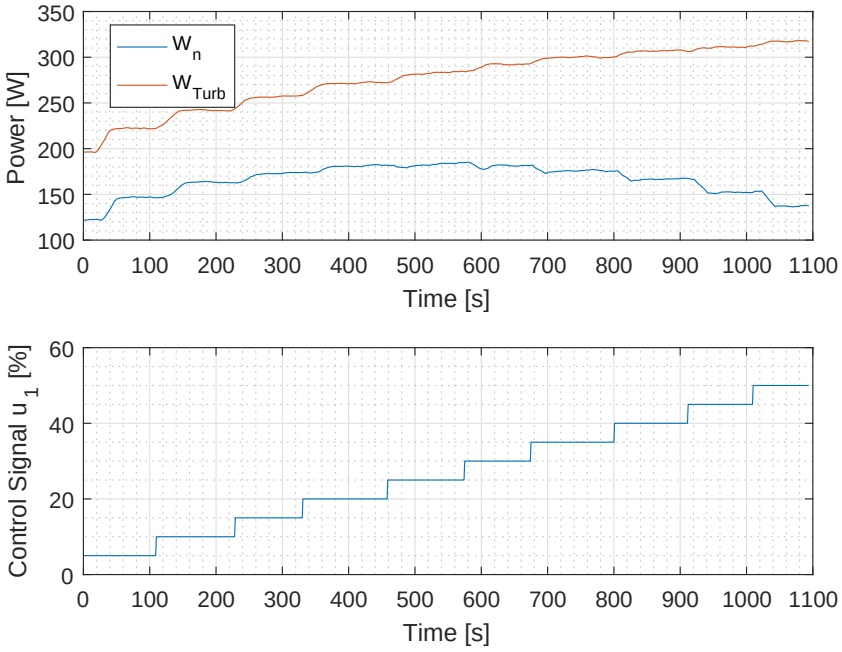

Figure 4-1: Response to step-wise increments on u_1 for fixed u_2

4-1-2 Step-Response u_1 and u_2

Both the control signals u_1 and u_2 are now varied in steps of 5%. Figure 4-2 shows how the performance of the plant varies due to these step-inputs. Using the steady-state values, a power map between u_1, u_2 and W_n is obtained. The power map in Figure 4-4 shows that there exists a specific combination of u_1 and u_2 that optimizes W_n. By analysing cross sections of the power map, W_n can be evaluated for a single input. The cross sections are shown in Figure 4-3. In Figure 4-3a, the power curve W_n is obtained for a fixed value $u_2 = 10\%$. In this situation, the maximum output $W_n \approx 156$W is obtained for a control signal of $u_1 \approx 20\%$. In Figure 4-3b the maximum output at $u_1 = 20\%$ is approximately 164W, for a control signal

$u_2 \approx 15\%$. These cross sections are used to test single parameter ESC, as discussed in the next section.

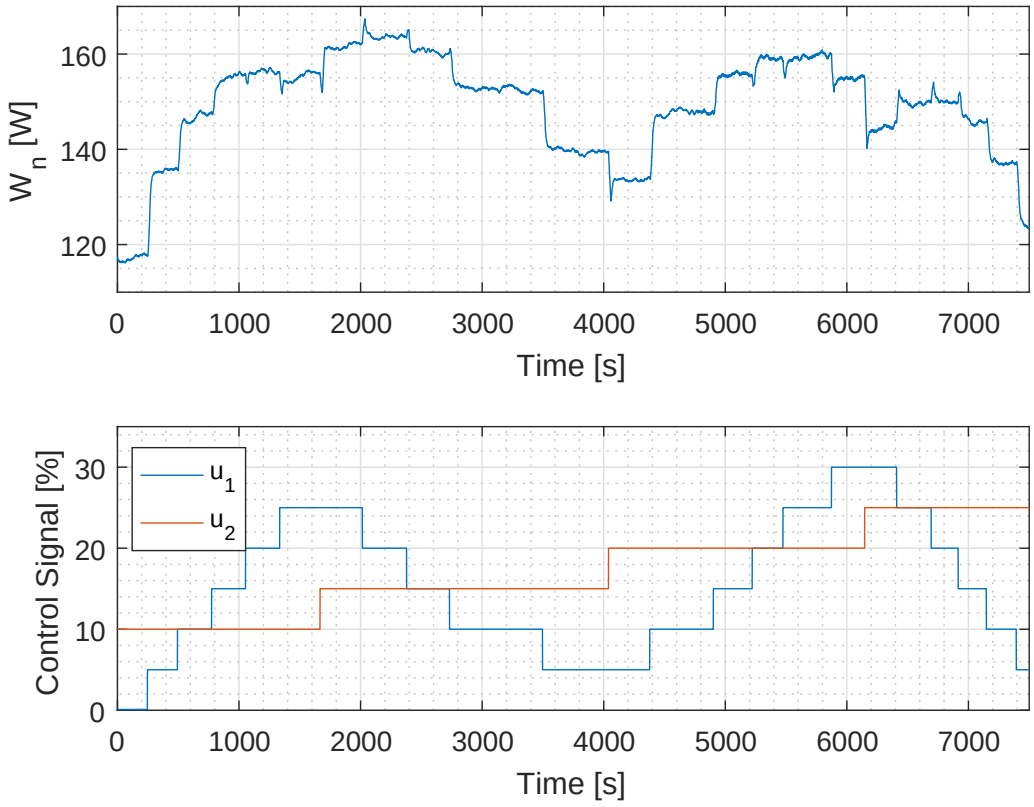

Figure 4-2: Response to steps on both u_1 and u_2

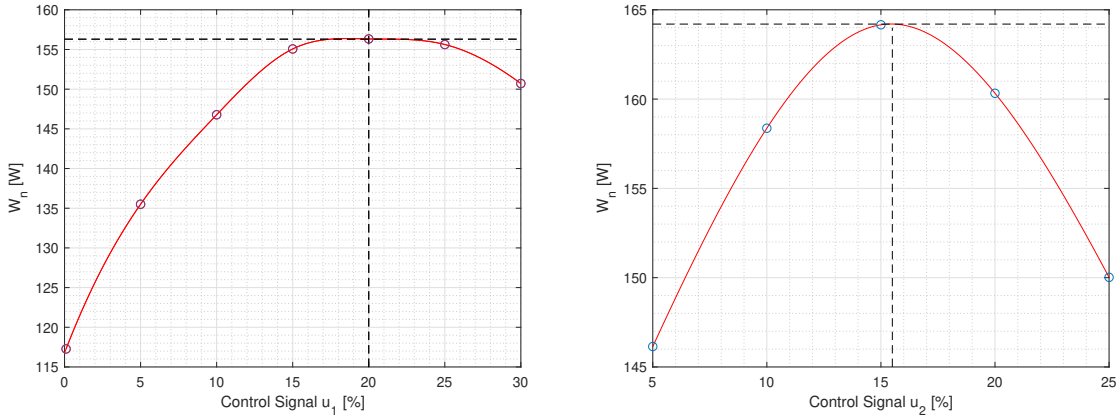

(a) Optimal u_1 for $u_2 = 10\%$ **(b)** Optimal u_2 for $u_1 = 20\%$

Figure 4-3: Optimal control signals u_1 and u_2

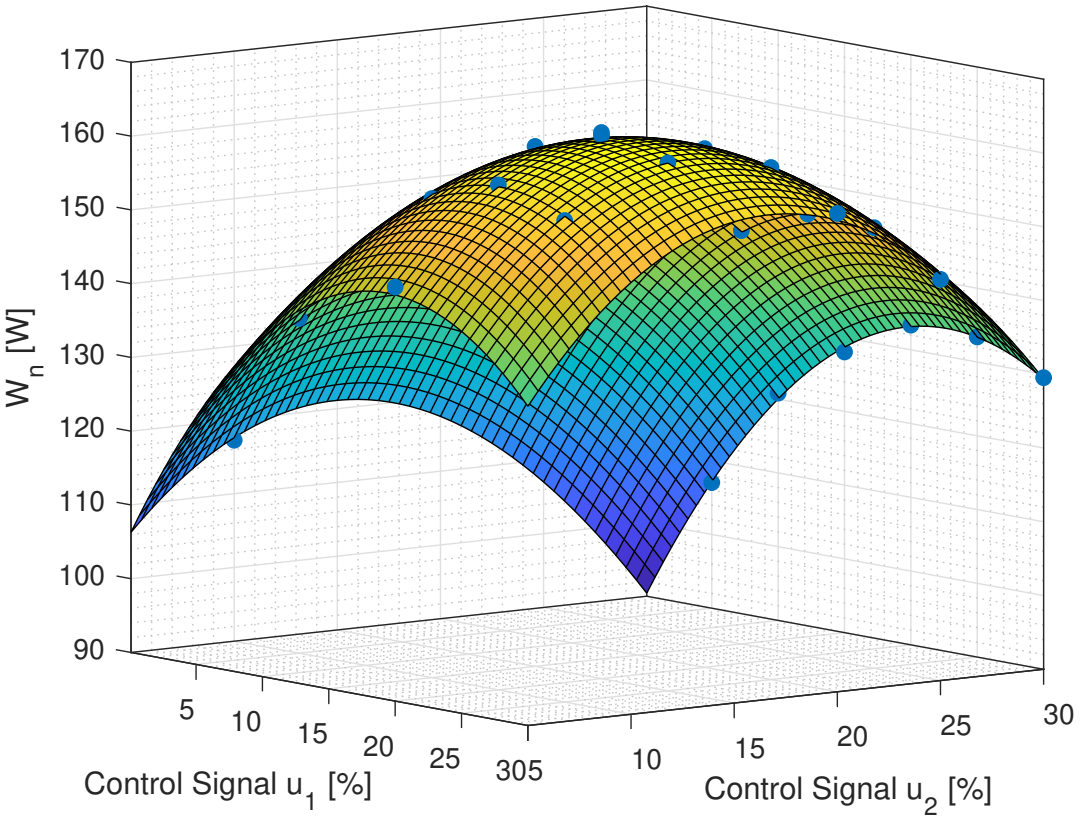

Figure 4-4: Power map between u_1, u_2 and W_n

4-2 Single Parameter ESC

4-2-1 ESC for u_1

In this experiment, single parameter ESC will be used to automatically find the optimal values that were estimated using the cross sections of the power map. Figure 4-3a showed that W_n reaches an optimum of approximately 156W, for a control signal u_1 of roughly 20%, when u_2 is kept constant at 10%. In section 3-2 is mentioned that is important to select the dither frequency ω within the bandwidth of the plant. Based on the step-responses from the previous experiment, ω is set to 0.01Hz. Figure 4-3a shows that W_n varies only slightly for u_1 between 15% and 25%. Hence, a small dither amplitude of 1% is selected. Different values of the adaptation gain k are investigated, varying between 0.01 and 0.03. The responses of this single parameter experiment are shown in Figure 4-5.

It was found that adaptation gains of $k > 0.03$ resulted in significant overshoot, while values of $k < 0.01$ resulted in a slow response. For $k = 0.015,\ 0.02,$ and 0.03 the response converges to an optimum close to the expected values, with no significant changes in speed of adaptation. The sensitivity to the adaptation gain confirms the findings from the simulation study. Figure 4-6 shows how the response can be improved further by reducing the dither amplitude to 0.5%. Compared to the situation with $a = 1\%$, the response with $a = 0.5\%$ displays a reduced undershoot. As expected, the perturbations are also less visible in W_n when the smaller dither amplitude is used.

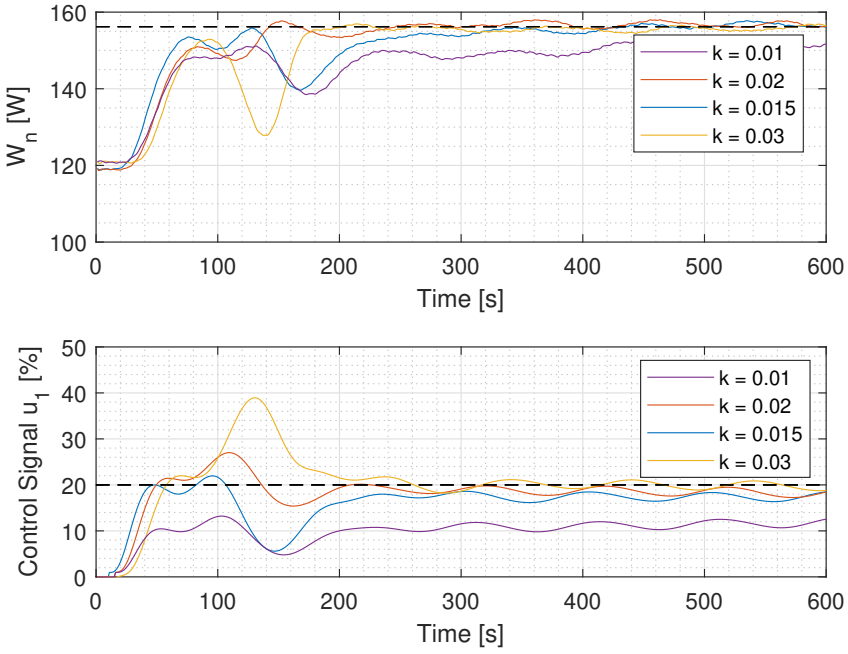

Figure 4-5: ESC applied to u_1 with different adaptation gains

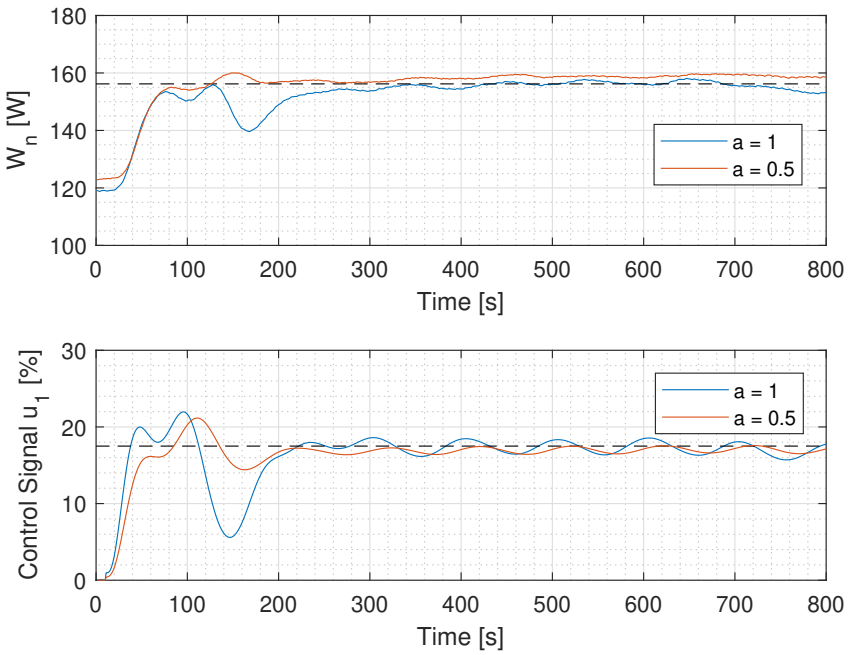

Figure 4-6: ESC for u_1, $\omega = 0.01$, $k = 0.02$

4-2-2 ESC for u_2

Here, ESC is used to optimize u_2, for a fixed value of u_1. Observing the cross section in Figure 4-3b, it is expected that an optimal power output of 164W is reached for an input of approximately 15%. The results are shown in Figure 4-7. Contrary to the results from section 4-2-1, the control signal does not seem to converge to the expected value. However, W_{net} does actually converge to the estimated optimum. This can be caused by the 'flatness' of the curve around the optimal inputs, indicated by the power map in Figure 4-4. Due to the shape of the curve, a wide range of inputs results in roughly the same power output. The response also shows a significant overshoot in the control signal, compared to the estimated optimum. This can be caused by a high adaptation gain, as was shown in Figure 4-5. It is recommended to repeat this experiment with a lower adaptation gain.

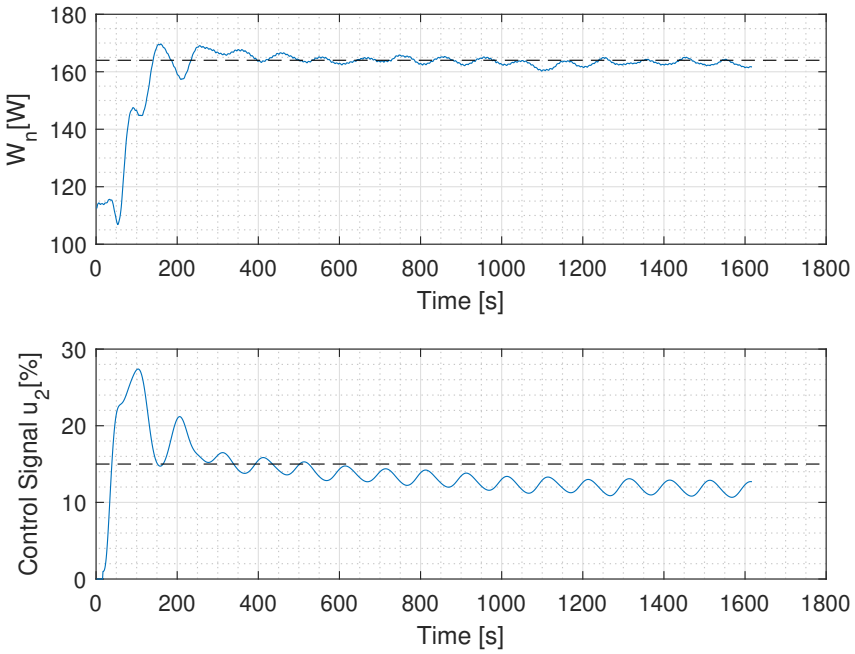

Figure 4-7: ESC for u_1, $a = 1$, $\omega = 0.01$, $k = 0.01$

4-3 Multivariable ESC

Multivariable ESC is used to optimize u_1 and u_2 simultaneously. As discussed in Section 3, it is important that the two dithers have distinct frequencies. The time responses of this experiment are shown in Figure 4-8. It is clear how u_1 and u_2 converge to distinct values. The value of W_n appears to approach that of the global optimum visualized in the power map in Figure 4-4. The trajectories are also visualized in Figure 4-9.

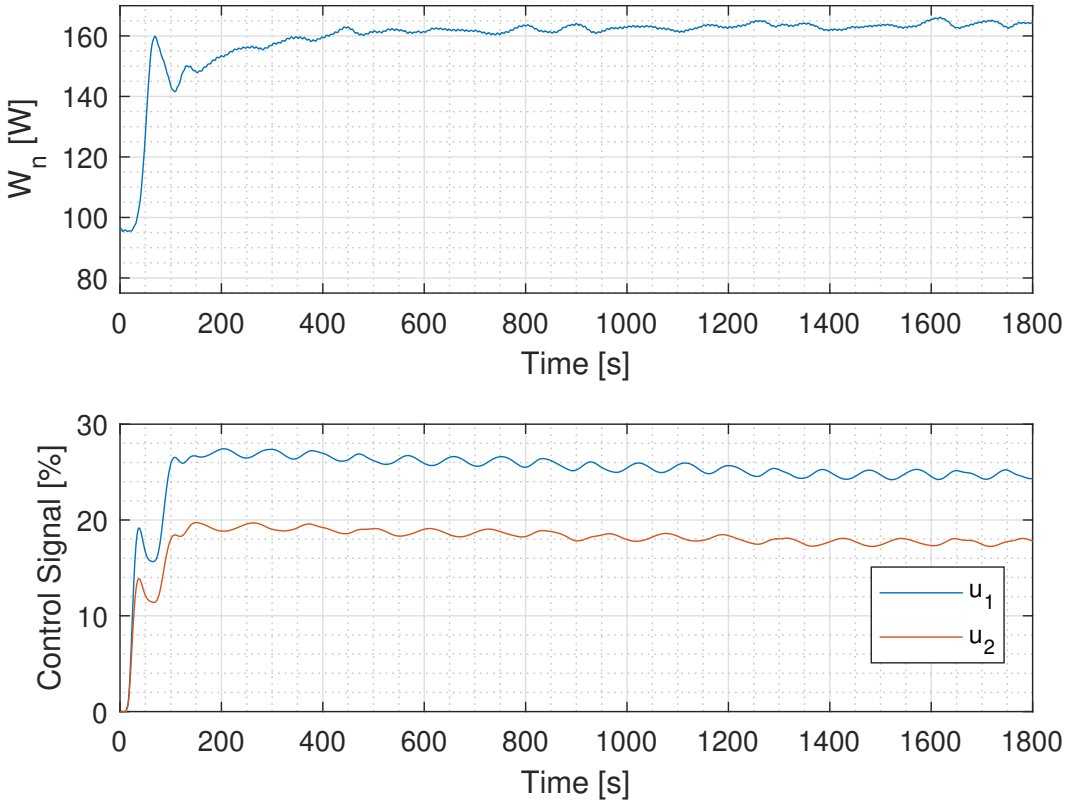

Figure 4-8: Multivariable ESC, $a_1 = 0.4$, $a_2 = 0.5$, $\omega_1 = 0.011$, $\omega_2 = 0.0083$ $k_1 = 0.025$, $k_2 = 0.015$

4-4 Discussion

A measurement of the cost function is obtained that has a sufficiently high signal to noise ratio to observe the trajectory around the optimum. The optimal inputs and corresponding performance are estimated by step-by-step increasing both control signals. By observing cross sections of the power map, the optimal inputs are estimated for fixed values of one the control signals. This information is used to verify the effectiveness of single parameter ESC. In the case of u_1, ESC is able to find the estsimated optimal value in roughly 250 seconds. The experiment for u_2 should be repeated for different tuning parameters. Multivariable ESC

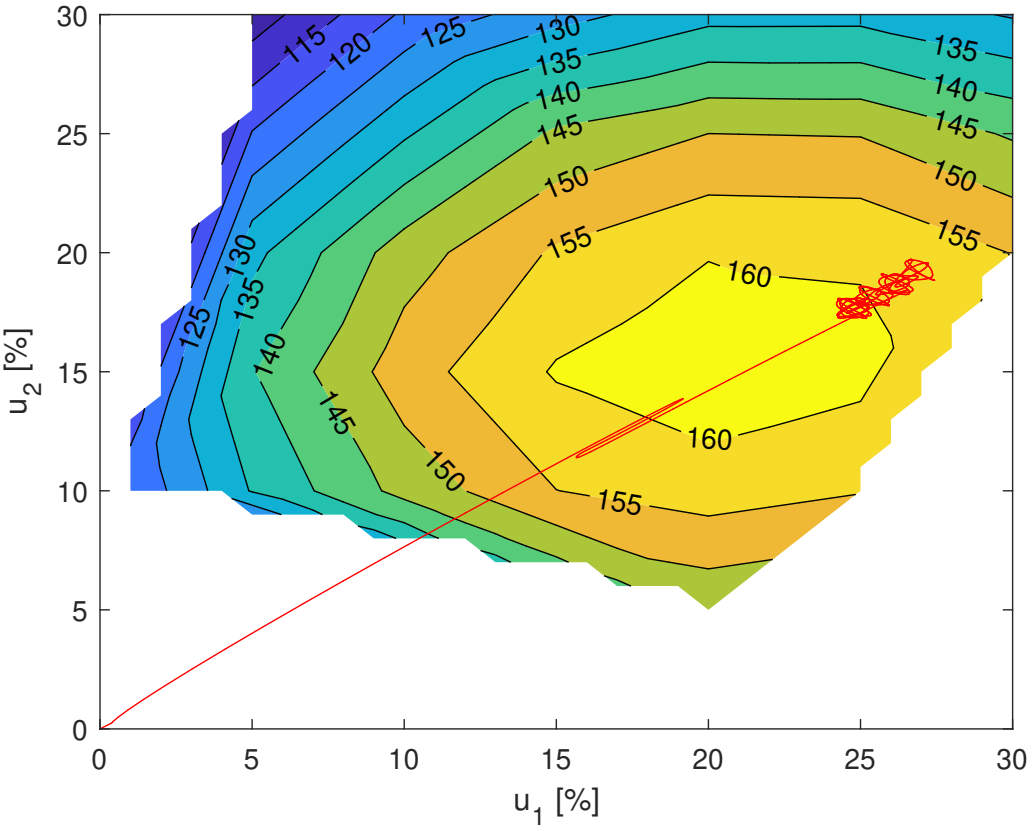

Figure 4-9: Trajectory of multivariable ESC

has been shown to be successful in optimizing both control signals simultaneously. It is also possible to reach the global optimum by optimizing the control signals individually, as can be seen by comparing the power output between the single parameter ESC and multivariable ESC.

Chapter 5

Conclusion & Recommendations

5-1 Conclusion

For OTEC to become commercially attractive, it is imperative to reduce the cost of electricity. The development of an effective control system can aid in this endeavor by making sure that the plant is operated at maximum capacity. The power generated in the turbine depends on the flow rates of warm and cold water, which can be controlled by varying the pump speed. However, the power consumption of the pumps will increase drastically when the flow rates are increased, resulting in a decreased net power output. Literature shows that the net power output of an OTEC power plant can be optimized by finding an optimal cold water flow rate.

Theoretically, the plant would operate at maximum capacity when an optimal cold water flow rate is used. However, due to modelling assumptions, this method can lead to suboptimal performance of the plant. Besides, performance of the plant varies over time as a result wear and tear, leakage of working fluid, and fluctuating ocean water temperatures. Comparable obstacles are encountered in maximizing the electricity production in wind turbines. A promising solution in this field is ESC.

For ESC to function properly, the mapping between the water flows and the net generated power should be concave. In literature, this is already shown to be the case for a model of a large scale plant. It has been demonstrated experimentally that such an optimum also exists for the OTEC-demo. The experiments have demonstrated that a similar optimum also exists for the warm water flow rate. By evaluating different combinations of the two control signals, a power map between the two control signals and the performance of the plant is constructed. By analysing cross sections of the power map, optimal values are estimated that are subsequently used to test the effectiveness of single parameter ESC.

First, single parameter ESC is tested by regulating the control signal u_1 of the warm water pump while the cold water flow is kept constant. It is shown that the system converges to the proximity of the optimal values that were estimated manually. The closed-loop performance is very sensitive to the adaptation gain, confirming the findings from the simulation. The controller was less successful in optimizing u_2. A downward trend could be observed in the

control signal. However, the output power converged to the expected value. The sensitivity to the adaptation gain k could be the culprit. It is recommended that this experiment is also repeated with different adaptation gains and dither frequencies.

To conclude, ESC is shown to be effective in automatically finding the set of inputs that optimize the power output of the OTEC-demo. On a more critical note, the tuning of the controller parameters was a very time-consuming task. So time-consuming that there is no direct time gain by using ESC, versus finding the optimal inputs manually. After each experiment the temperatures of the water reservoirs had to be warmed or cooled to their initial temperatures. This will of course not be the case in an actual plant. Besides, during the experiments the control signals started from an initial value equal to zero. It is expected that the speed of adaptation can be increased by setting the initial control signals closer to the expected optima. These can be obtained using models of the plant, or from operational data.

5-2 Recommendations

This study has focused on the implementation of the basic ESC-algorithm to both the water pumps. The current LabVIEW implementation is also ready to be used to optimize the working fluid flow rate. This is not done during this study, because of the intricate interaction between the working fluid pump frequency and the working fluid flow rate, as explained in Appendix A.

When the OTEC-demo is fitted with a turbine, it would be interesting to optimize for electrical power, instead of the mechanical power output. Speculating on future improvements of the OTEC-demo, the ammonia concentration could also be used as a control input.

It would be interesting to investigate how the algorithm performs when subjected to fluctuations in the water temperature, as will be the case in actual power plants.

Since ESC uses standard elements like low-pass filters and high-pass filters, the algorithm can easily be extended to a plant of industrial scale. Also on a larger plant, the tuning parameters can be selected based on step-response data. In a larger plant, the cost function can be measured by directly measuring the electric power generated in the turbine, and the electric power consumed by the pumps.

ESC could also be of worth to other Bluerise projects. For example, the yield of the Ocean Thermal Water Production (OTWP) plant can be optimized by using ESC to regulate the air flows and water flows.

Appendix A

Details on the implementation

A-1 Measuring the cost function

The net mechanical power generated in the OTEC-demo is given by Equation 2-6. Here, W_n depends on the measurements given by 2-7. This signal should have a sufficiently high signal-to-noise ratio, such that small changes in the control signal can be observed in the output. That this is not the case for the unprocessed signal, is shown in Figure A-1a. Figure A-1b shows how the signal improves when a moving average filter is used to filter the measurements. As expected, the filter is capable of removing the majority of the noise. However, the quality of the signal is still too low to investigate the behaviour around the optimum.

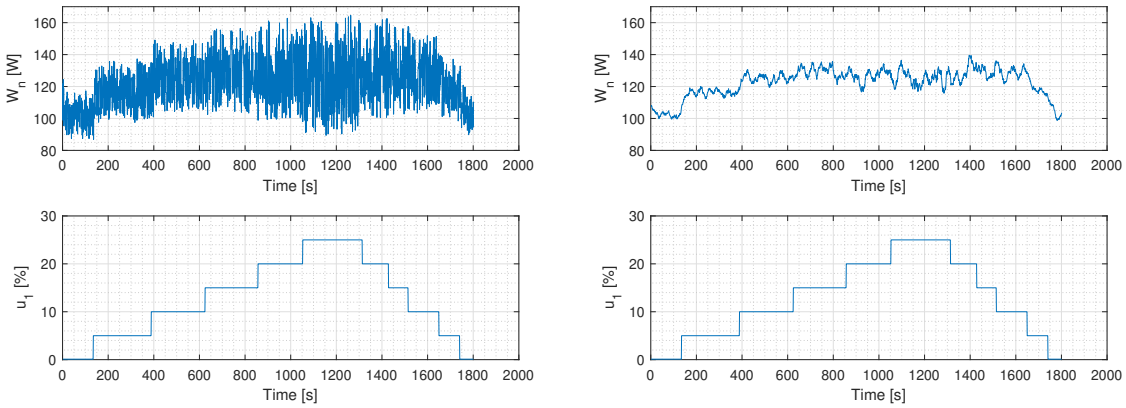

(a) Unprocessed cost function

(b) MA-filtered output (20 samples)

Figure A-1: Results of implementing a moving average filter on the cost function

Besides filtering the output, the signal quality can also be improved by addressing the source of the noise. The mechanical power of the water pumps depends on the water flow rate and the pressure at the inlet and outlet of the pump. The power consumption of the water pumps

is shown in Figure A-4a. The signal belonging to the warm water pump is noisy compared to the signal of the cold water pump. According to Equation 2-3, the power consumption of the water pumps depends on the pressure difference between the inlet and outlet. The pressures at the inlets and the outlets of the pumps are inspected individually, as shown in Figure A-4b. It becomes clear that the signal originating from sensor PI-22, measuring the inlet pressure of the warm water pump, is the culprit.

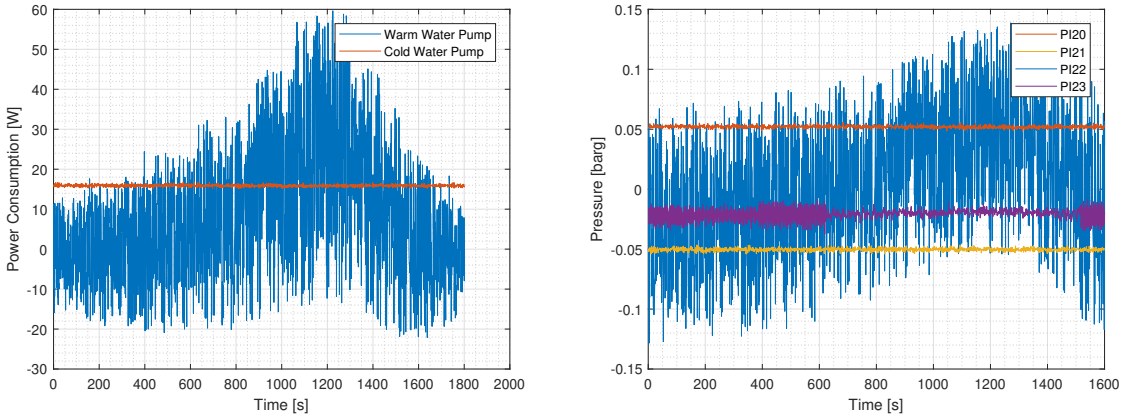

(a) Water Pumps Power Consumption **(b)** Pressure measurements

Figure A-2: adfadf

The so-called pump affinity laws state that the power consumption of the pumps is proportional to the third power of the mass flow rate, and the mass flow rate is proportional to the velocity of the pump [5]. Due to the linear input-output relation of variable frequency drives, there exists a linear relationship between the control signal and the pump velocity. The control signal of the water pumps varies between 0 and 100 %, corresponding to a velocity between 20 and 50Hz. To prevent the noisy measurements of the power consumption from interfering with the evaluation of the performance index, a function is determined that directly relates the control signal of the water pumps to their power consumption. Figure A-5 clearly illustrates how the power consumption of the water pump is proportional to the third power of the control signal. Figure A-4a and Figure A-4b demonstrate how the estimated power consumption compares to the measured power consumption. The improvement is especially clear in Figure A-4a. Relating the mechanical power consumption directly to the control signal was required to deal with the noise levels in the pressure sensor.

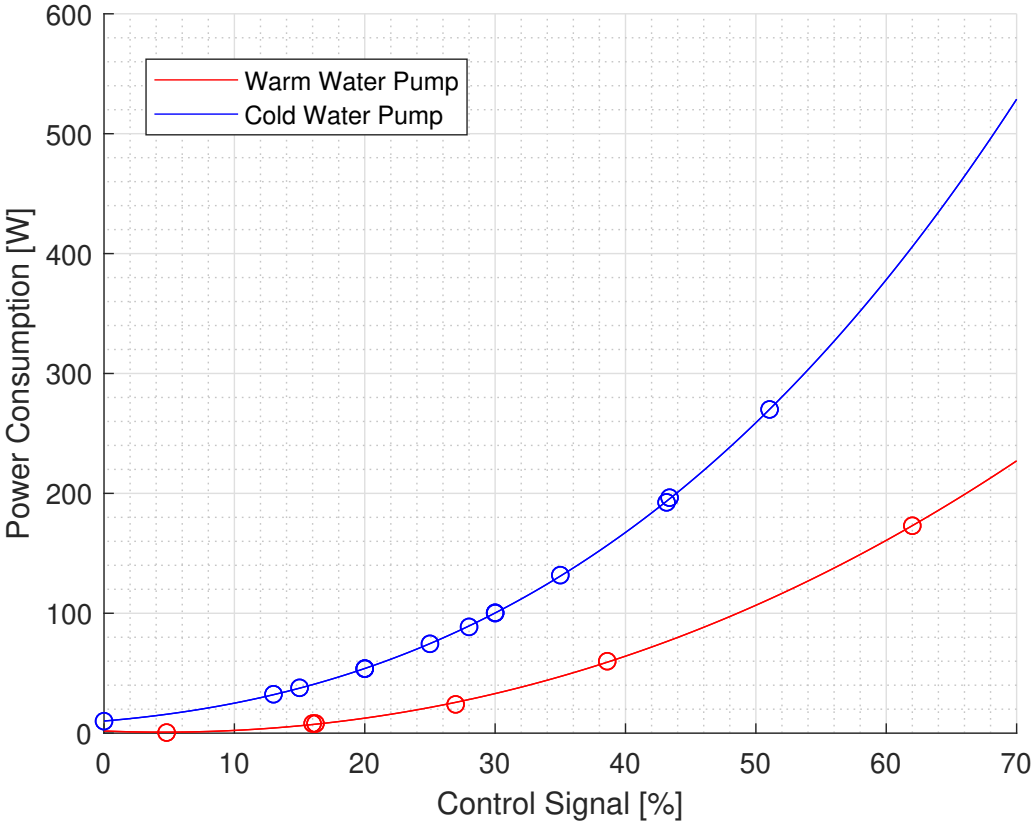

Figure A-3: Power consumptions of water pumps for different water flows

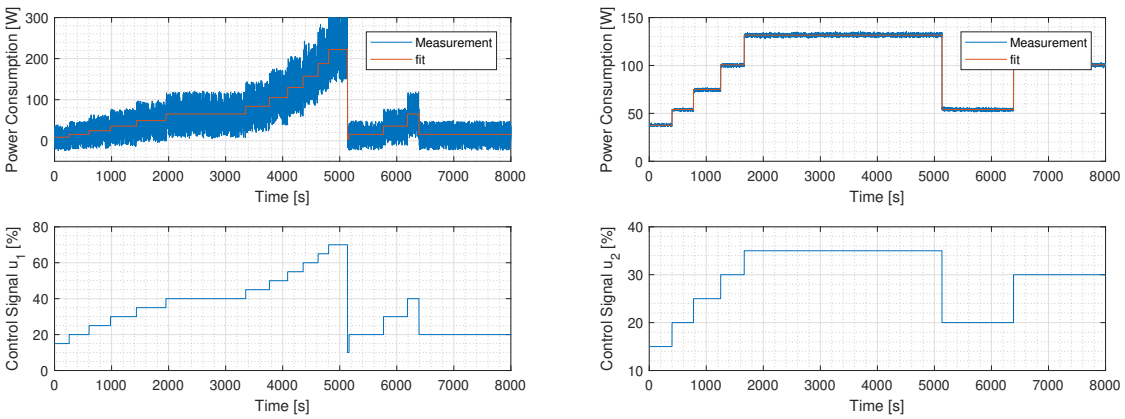

(a) P2 estimated power consumption

(b) P3 estimated power consumption

A-2 Process noise

Besides dealing with measurement noise, there is also a source of noise in the process itself. As shown in Figure A-5 , the working fluid flow rate at the exit of the pump displays an oscillatory character, caused by the reciprocating action of the diaphragm pump. The oscillations can be reduced by properly adjusting the damper. Initally, the valve is fully opened. The valve is then gruadually closed, while observing the real-time data feed. It is clear how this improves the flow rate around the 700s and 1000s mark. The amplitude of the oscillations is drastically reduced, but the periodic behavior is still clearly visible. The damper appears to be working better for increased flow rates, judging by the improvements following the increased control signal around the 1600s mark. Due to the fact that the amount of oscillations in the working fluid is so dependent on the working fluid pump speed, the working fluid pump speed is kept constant during this study, and thus not used as input for the ESC experiments.

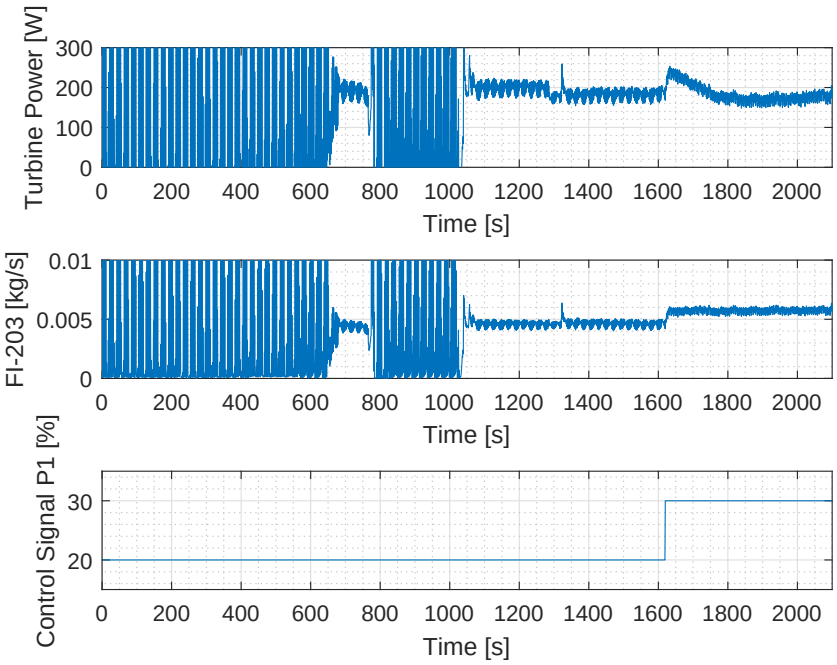

Figure A-5: Effects of valve-opening and control signal

A-3 Performance Improvement

To summarize, three improvements are made to the measurement of the cost function. The signal is filtered by using a moving average filter, the power consumption is now estimated by using a polynomial function of the control signal, and the oscillations in the turbine power can be reduced by properly tuning the damper and adjusting the working fluid pump speed accordingly. The results of these improvements are shown in Figure A-6. The influence of the control signal is now clearly visible in the output.

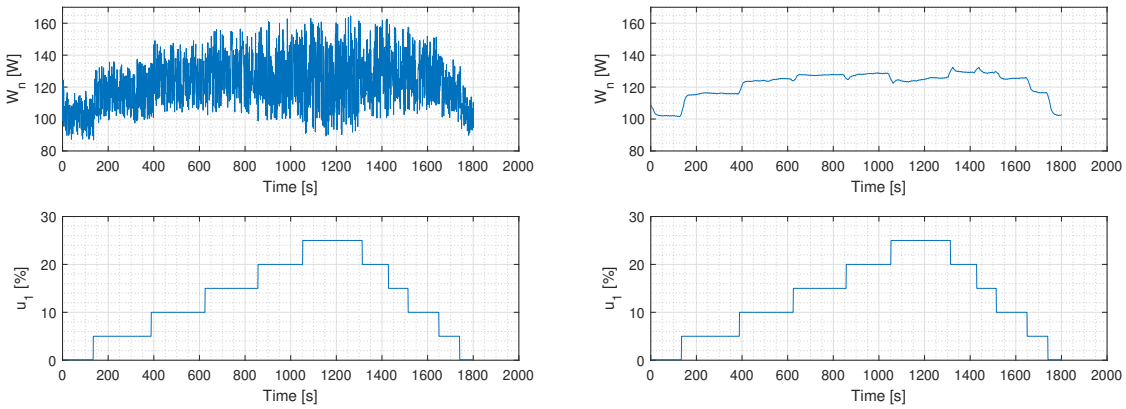

(a) Unprocessed cost function

(b) Processed cost function

Figure A-6: Results of addressing the noise sources

Bibliography

[1] Alireza Khaligh and Omer C Onar. "Ocean Thermal Energy Harvesting". In: *Energy Harvesting: Solar, Wind, and Ocean Energy Conversion Systems*. CRC Press, 2009. Chap. Chapter 5. Pp. 305–341. ISBN: 978-1-4398-1509-0.

[2] Ahmet Apak et al. "Design and Construction of an Ocean Thermal Energy Conversion Test Plant". In: 102141.February 1980 (1980), pp. 84–89.

[3] Kartik B Ariyur and Miroslav Krstić. "Analysis and design of multivariable extremum seeking". In: *Proceedings of the American Control Conference* 4.0 (2002), pp. 2903–2908. ISSN: 07431619. DOI: 10.1109/ACC.2002.1025231.

[4] Bluerise BV. *Offshore ocean thermal energy conversion; Feasibility study of a 10 MW installation*. Tech. rep. March. 2014, p. 64.

[5] Carrier. "Variable Frequency Drive". In: *New York* October (2005), p. 11.

[6] Justin Creaby, Yaoyu Li, and John E Seem. "Maximizing Wind Turbine Energy Capture using Multivariable Extremum Seeking Control". In: *Wind Engineering* 33 (2009), pp. 361–387. ISSN: 0309-524X. DOI: 10.1260/030952409789685753.

[7] M.E. Dahlgren. "Experimental study of transport phenomena in the condenser of an OTEC-Cycle". PhD thesis. Delft University of Technology, 2018.

[8] Judith Ebegbulem and Martin Guay. "Distributed Extremum Seeking Control for Wind Farm Power Maximization". In: 2012 (2017).

[9] Mohammed Faizal and M. Rafiuddin Ahmed. "On the ocean heat budget and ocean thermal energy conversion". In: *International journal of Energy Research* 35.July (2011), pp. 1119–1144. ISSN: 12310956. DOI: 10.1002/er. arXiv: arXiv:1011.1669v3.

[10] Azad Ghaffari, Miroslav Krstić, and Sridhar Seshagiri. "Power optimization and control in wind energy conversion systems using extremum seeking". In: *IEEE Transactions on Control Systems Technology* 22.5 (2014), pp. 1684–1695. ISSN: 10636536. DOI: 10.1109/TCST.2014.2303112.

[11] Satoru Goto et al. "Controller Design for OTEC Experimental Pilot Plant Based on Nonlinear Separation Control". In: *SICE Annual Conference 2004*. 2004, pp. 879–884.

[12] Martin Guay and Daniel J. Burns. "A comparison of extremum seeking algorithms applied to vapor compression system optimization". In: *Proceedings of the American Control Conference* (2014), pp. 1076–1081. ISSN: 07431619. DOI: 10.1109/ACC.2014.6859288.

[13] V Gudjonsdottir. "Analysis of external influences on an OTEC cycle". PhD thesis. Delft University of Technology, 2015.

[14] A W Harmsen. "Improving, testing and verification of a small-scale OTEC research plant". In: (2016).

[15] Andres Hernandez et al. "Real-Time Optimization of Organic Rankine Cycle Systems by Extremum-Seeking Control". In: *Energies* 9.5 (2016), p. 334. ISSN: 1996-1073. DOI: 10.3390/en9050334. URL: http://www.mdpi.com/1996-1073/9/5/334.

[16] Henry Johnson, David; Mlcak. "The Husavik Kalina Cycle Control System". In: *Geothermal Resources Council Transactions* 26 (2002), pp. 731–734. URL: https://www.geothermal-library.org/index.php?mode=pubs%7B%5C&%7Daction=view%7B%5C&%7Drecord=1019689.

[17] Kathryn E. Johnson et al. "Methods for Increasing Region 2 Power Capture on a Variable-Speed Wind Turbine". In: *Journal of Solar Energy Engineering* 126.4 (2004), p. 1092. ISSN: 01996231. DOI: 10.1115/1.1792653. URL: http://solarenergyengineering.asmedigitalcollection.asme.org/article.aspx?articleid=1457167.

[18] A I Kalina. "Combined-Cycle System With Novel Bottoming Cycle". In: *Journal of Engineering for Gas Turbines and Power* 106.October 1984 (1984), pp. 737–742.

[19] B J Kleute. "System sensitivity and cold water pipe analysis of a 10 MW offshore OTEC - ocean thermal energy conversion plant". In: (2014).

[20] Justin P. Koeln and Andrew G. Alleyne. "Optimal subcooling in vapor compression systems via extremum seeking control: Theory and experiments". In: *International Journal of Refrigeration* 43 (2014), pp. 14–25. ISSN: 01407007. DOI: 10.1016/j.ijrefrig.2014.03.012. URL: http://dx.doi.org/10.1016/j.ijrefrig.2014.03.012.

[21] Miroslav Krstić. "Performance improvement and limitations in extremum seeking control". In: *Systems & Control Letters* 39.5 (2000), pp. 313–326. ISSN: 01676911. DOI: 10.1016/S0167-6911(99)00111-5.

[22] Miroslav Krstić. "Performance improvement and limitations in extremum seeking control". In: *Systems & Control Letters* 39.5 (2000), pp. 313–326. ISSN: 01676911. DOI: 10.1016/S0167-6911(99)00111-5.

[23] Miroslav Krstic, Azad Ghaffari, and Sridhar Seshagiri. "Extremum seeking for wind and solar energy applications". In: *Proceeding of the 11th World Congress on Intelligent Control and Automation* (2014), pp. 6184–6193. DOI: 10.1109/WCICA.2014.7053780. URL: http://ieeexplore.ieee.org/document/7053780/.

[24] L J Kuikhoven. "Influence of the ammonia concentration on the performance of OTEC power cycles". In: ().

[25] Christophe Labar, Emanuele Garone, and Michel Kinnaert. "Sub-Optimal Extremum Seeking Control". In: (2017), pp. 8028–8034.

[26] M. LEBLANC. "Sur l'electrification des chemins de fer au moyen de courants alternatifs de frequence elevee". In: *Revue Generale de l'Electricite* 12.8 (1922), pp. 275–277. URL: https://ci.nii.ac.jp/naid/10017139032/en/.

[27] R Leyva et al. "MPPT of photovoltaic systems using extremum-seeking control". In: *Ieee Transactions on Aerospace and Electronic Systems* 42.1 (2006), pp. 249–258. ISSN: 0018-9251. DOI: 10.1109/taes.2006.1603420.

[28] Chris Manzie and Miroslav Krstic. "Extremum seeking with stochastic perturbations". In: *IEEE Transactions on Automatic Control* 54.3 (2009), pp. 580–585. ISSN: 00189286. DOI: 10.1109/TAC.2008.2008320.

[29] Yoshitaka Matsuda et al. "Control of OTEC Plant Using Double-stage Rankine Cycle Considering Warm Seawater Temperature Variation". In: (2016).

[30] H.A. Mlcak. "Kalina Cycle Concepts for Low Temperature Geothermal". In: *Geothermal Resources Council Transactions* (2002), pp. 707–711. ISSN: 01935933.

[31] Baojie Mu et al. "Experimental evaluation of anti-windup extremum seeking control for airside economizers". In: *Control Engineering Practice* 50 (2016), pp. 37–47. ISSN: 09670661. DOI: 10.1016/j.conengprac.2016.02.008. URL: http://dx.doi.org/10.1016/j.conengprac.2016.02.008.

[32] Carlos Olalla et al. "Analysis and Comparison of Extremum Seeking Control Techniques". In: *2007 IEEE International Symposium on Industrial Electronics* 3 (2007), pp. 72–76. DOI: 10.1109/ISIE.2007.4374576.

[33] W L Owens. "OTEC Plant Response and Control Analysis". In: *Journal of Solar Energy Engineering* 104.August (1982).

[34] Mario A Rotea. "Logarithmic Power Feedback for Extremum Seeking Control of Wind Turbines". In: (2017), pp. 4590–4595.

[35] Faming Sun and Yasuyuki Ikegami. "Direct Method to Maximize Net Power Output of Rankine Cycle in Low-Grade Thermal Energy Conversion". In: *Journal of Thermal Science and Engineering Applications* 2.2 (2010), p. 021003. ISSN: 19485085. DOI: 10.1115/1.4002564. URL: http://thermalscienceapplication.asmedigitalcollection.asme.org/article.aspx?articleid=1469440.

[36] Faming Sun et al. "Optimization design and exergy analysis of organic rankine cycle in ocean thermal energy conversion". In: *Applied Ocean Research* 35 (2012), pp. 38–46. ISSN: 01411187. DOI: 10.1016/j.apor.2011.12.006. URL: http://dx.doi.org/10.1016/j.apor.2011.12.006.

[37] Ying Tan, Dragan Nešić, and Iven Mareels. "On the choice of dither in extremum seeking systems: A case study". In: *Automatica* 44.5 (2008), pp. 1446–1450. ISSN: 00051098. DOI: 10.1016/j.automatica.2007.10.016.

[38] Haruo Uehara and Yasuyuki Ikegami. "Optimization of a Closed-Cycle OTEC System". In: 112.June 1990 (1990), pp. 247–256.

[39] L Vega. "The 210 kW Open Cycle OTEC Experimental Apparatus: status report". In: *'Challenges of Our Changing Global Environment'. Conference Proceedings. OCEANS '95 MTS/IEEE* 2 (1995), pp. 1110–1115. ISSN: 01977385. DOI: 10.1109/OCEANS.1995.528580. URL: http://ieeexplore.ieee.org/lpdocs/epic03/wrapper.htm?arnumber=528580.

[40] Luis A. Vega. "Ocean Thermal Energy Conversion". In: *Encyclopedia of Sustainability Science and Technology*. Ed. by Robert A. Meyers. New York: Springer, 2012. Chap. Ocean Ther, pp. 7296–7327. ISBN: 978-0-387-89469-0. DOI: 10.1007/978-1-4419-0851-3. arXiv: UCD-ITS-RR-09-08. URL: http://link.springer.com/10.1007/978-1-4419-0851-3.

[41] Luis A. Vega. "Ocean Thermal Energy Conversion". In: *Encyclopedia of Sustainability Science and Technology* 36.4 (2012), pp. 2796–7328. ISSN: 00253324. DOI: 10.4031/002533202787908626.

[42] Robert Van Der Weijst and Thijs Van Keulen. "A generalized framework for perturbation-based derivative estimation in multivariable extremum-seeking". In: (2017), pp. 3203–3208.

[43] Chih Wu. "Specific power optimization of closed-cycle OTEC plants". In: *Ocean Engineering* 17.3 (1990), pp. 307–314. ISSN: 00298018. DOI: 10.1016/0029-8018(90)90007-S.

[44] Min-Hsiung Yang and Rong-Hua Yeh. "Analysis of optimization in an OTEC plant using organic Rankine cycle". In: *Renewable Energy* 68 (2014), pp. 25–34. ISSN: 09601481. DOI: 10.1016/j.renene.2014.01.029. URL: http://linkinghub.elsevier.com/retrieve/pii/S0960148114000585%20http://www.sciencedirect.com/science/article/pii/S0960148114000585.

[45] Zhongzhou Yang, Yaoyu Li, and John E Seem. "Optimizing Energy Capture of Cascaded Wind Turbine Array With Nested-Loop Extremum Seeking Control". In: *Journal of Dynamic Systems, Measurement, and Control* 137.12 (2015), p. 121010. ISSN: 0022-0434. DOI: 10.1115/1.4031593. URL: http://dynamicsystems.asmedigitalcollection.asme.org/article.aspx?doi=10.1115/1.4031593.

[46] Her-Terng Yau and Chen-Han Wu. "Comparison of Extremum-Seeking Control Techniques for Maximum Power Point Tracking in Photovoltaic Systems". In: *Energies* 4.12 (2011), pp. 2180–2195. ISSN: 1996-1073. DOI: 10.3390/en4122180. URL: http://www.mdpi.com/1996-1073/4/12/2180/.

[47] Rong Hua Yeh, Tar Zen Su, and Min Shong Yang. "Maximum output of an OTEC power plant". In: *Ocean Engineering* 32.5-6 (2005), pp. 685–700. ISSN: 00298018. DOI: 10.1016/j.oceaneng.2004.08.011.

[48] Xinxin Zhang, Maogang He, and Ying Zhang. "A review of research on the Kalina cycle". In: *Renewable and Sustainable Energy Reviews* 16.7 (2012), pp. 5309–5318. ISSN: 13640321. DOI: 10.1016/j.rser.2012.05.040. URL: http://dx.doi.org/10.1016/j.rser.2012.05.040.

Glossary

List of Acronyms

OTEC	Ocean Thermal Energy Conversion
SIDS	Small Island Development States
TU Delft	Delft University of Technology
ORC	Organic Rankine Cycle
LCOE	Levelized Cost of electricity
ESC	Extremum Seeking Control
MPPT	Maximum Power Point Tracking
VI	Virtual Instrument
OTWP	Ocean Thermal Water Production